5 Numerical Renormalization Group and Multi-Orbital Kondo Physics

T.A. Costi
Institute for Advanced Simulation (IAS-3)
Forschungszentrum Jülich

Contents

E. Pavarini, E. Koch, and P. Coleman (eds.)
Many-Body Physics: From Kondo to Hubbard
Modeling and Simulation Vol. 5
Forschungszentrum Jülich, 2015, ISBN 978-3-95806-074-6
http://www.cond-mat.de/events/correl15

1 Introduction

This lecture deals with a particular implementation of the renormalization group idea: Wilson's non-perturbative numerical renormalization group (NRG) method for quantum impurity models [1]. The technique was originally developed in the context of the Kondo model for magnetic impurities (such as Fe or Mn) in non-magnetic metals (such as Cu, Au, Ag etc).
The Kondo model is defined by the Hamiltonian

$$H_{\rm KM} = J\,\vec{S}\cdot\vec{s}_0 + \sum_{k\sigma}\varepsilon_{k\sigma}\,c^\dagger_{k\sigma}c_{k\sigma}\,, \tag{1}$$

and describes a localized impurity spin $\vec{S}$ interacting antiferromagnetically ($J > 0$) with the conduction electrons of the host via their spin density $\vec{s}_0$ at the impurity site. Unlike the case of non-magnetic impurities, or potential scatterers, magnetic impurities have internal dynamical degrees of freedom that result in inelastic scattering of conduction electrons. This makes the Kondo problem, the scattering of electrons from magnetic impurities, a genuine many-body correlation problem. Wilson used the NRG to solve the many-body Hamiltonian (1) and demonstrated conclusively that a $S = 1/2$ magnetic impurity embedded in a non-magnetic metal has its magnetic moment completely screened by the surrounding conduction electrons, provided the temperature is sufficiently low, namely for $T \ll T_K$, where $T_K = \sqrt{JN_{\rm F}}\,e^{-1/JN_{\rm F}}$ is a dynamically generated low-energy scale called the Kondo scale (see Sec. 2). This pioneering work established the formalism and gave a detailed analysis of the fixed points and thermodynamics of the Kondo model and, later, also of the Anderson impurity model. The NRG has since been applied to many more quantum impurity models [2–4]. In addition, it has been extended to the calculation of equilibrium dynamical and transport properties [5–10], e.g., dynamical susceptibilities, resistivities and thermopower or the conductance through quantum dots [11], thereby making the NRG a useful tool for interpreting experiments that probe these quantities.
Despite this progress, the NRG is still under development, and important challenges remain to be addressed. Two such challenges are (i) to extend it to more realistic multi-orbital and multi-channel models (e.g., for use in realistic modeling of materials), and (ii) to extend it to the transient and non-equilibrium steady state response of quantum impurity systems. Recent progress and ideas in these two directions are outlined in Sec. 6.
The outline of this lecture is as follows: Quantum impurity models are introduced in Sec. 2; the linear chain representation of such models is described, and the first step in the NRG procedure is also indicated there (the "zeroth approximation"). Anderson impurity and Kondo models are described, as is the spin-boson model and its fermionic equivalents: the anisotropic Kondo model (AKM) and the interacting resonant level model (IRLM). For a direct treatment of bosonic models within NRG, see the Lecture by K. Ingersent.
Wilson's NRG method is described in Sec. 3, and the calculation of physical properties is outlined in Sec. 4. In Sec. 5, we describe the recently introduced complete basis set [12] and its use in constructing the full density matrix [10]. Applications to thermodynamics and Green functions are given. An outline of some recent developments using the NRG is given in Sec. 6, and Sec. 7 summarizes with possible future directions.

2 Quantum impurity models

Quantum impurity models describe systems where the many-body interaction acts at one or only a few sites, the "impurity," and the impurity is coupled to a large system, the bath, consisting of a macroscopically large number of non-interacting particles. These particles can be either bosons (e.g., phonons, magnons, photons, particle-hole pairs, etc.) or fermions (e.g., electrons in the conduction band or quasiparticles in superconductors). The "impurity" may be a real impurity, such as an Fe impurity (in Au), or a two-level atom (coupled to the electromagnetic field), or just a confined region behaving like an artificial atom, as in the case of semiconductor quantum dots (coupled to leads). It may also simply represent the lowest two quantum mechanical states of a system with a double-well potential, as in the case of quantum tunneling between macroscopic fluxoid states in a superconducting quantum interference device, which can be used to realize a qubit for quantum computation. Two magnetic impurities in a non-magnetic metal at a distance R apart, interacting via the RKKY indirect exchange $J_{\rm RKKY}$ may also be regarded as a quantum impurity system [13]. Analogues of this in nanostructures, such as double quantum dots attached to leads, also exist. The transfer of electrons between donor and acceptor molecules in photosynthesis and other biological processes may also be crudely described in terms of a two-state system coupled to environmental degrees of freedom (solvent). Concrete models describing the above situations go under the names of (isotropic and anisotropic) single and multi-channel Kondo models, the Anderson impurity model, and the dissipative two-state system [14, 15]. They describe a large number of physical systems of current experimental and theoretical interest. Quantum impurity models are also of relevance in the study of correlated lattice models, such as the Hubbard or Kondo lattice models, since the latter are often well approximated, via the dynamical mean-field theory, by a local impurity model embedded in a medium that has to be determined self-consistently [16].

Historically, interest in quantum impurities arose when magnetic impurities were found to be present, albeit in very low concentrations, even in apparently very pure metals such as Au or Ag. In particular, measurements of the resistivity of Au as early as the 1930's showed an unexpected minimum at low temperature (Fig. 1). The puzzle of the resistivity minimum was resolved by Kondo in 1964, who showed that a small concentration $c_{\rm imp}$ of *magnetic* impurities modeled by Eq. (1) gives rise to an additional temperature dependent term in the resistivity of the form $\rho_{\rm K} = -c_{\rm imp}\, b\, \ln(T/D)$, which increases with decreasing temperature. The balance between the decreasing phonon contribution behaving as $\rho_{\rm phonon} = aT^5$ and the increasing Kondo contribution gives rise to the observed resistivity minimum. The logarithmic contribution to the resistivity, found by Kondo in perturbation theory, cannot hold down to $T = 0$ as the total scattering remains finite in this limit (unitarity limit). Wilson's non-perturbative NRG provides a way to obtain the correct behavior of the resistivity $\rho(T)$ from high temperatures through a crossover regime at $T \sim T_{\rm K}$ all the way down to zero temperature [see Fig. 11a showing the analogous quantity for a Kondo correlated quantum dot, the conductance $G(T)$].

The general form of the Hamiltonian for any quantum impurity system is given by

$$H = H_{\rm imp} + H_{\rm int} + H_{\rm bath}\,, \tag{2}$$

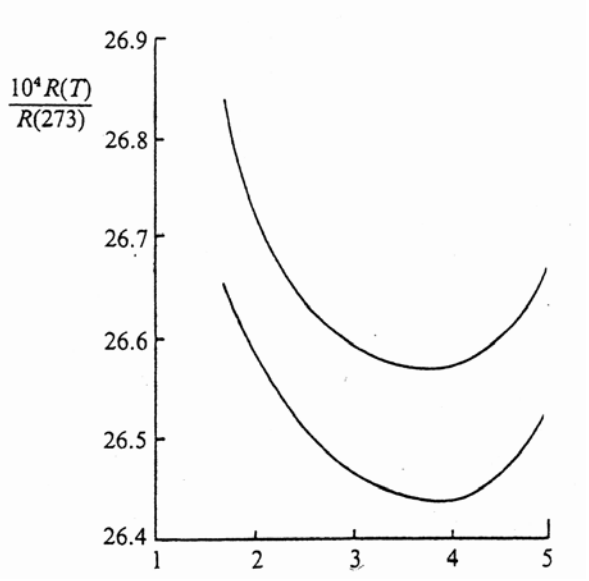

Fig. 1: *Resistivity $R(T)$ versus temperature $T[K]$ of two samples of "pure"* Au *showing the first observation of the resistivity minimum [17]. The expected behavior of $R(T)$ for a pure metal with weak static disorder is a T^5 term due to phonons and a saturation to a constant value, ρ_0, at $T = 0$ due to static disorder. The former is seen in the experiment, but at low temperature an additional logarithmically increasing contribution is also found.*

where $H_{\rm imp}$ describes the impurity, a small quantum mechanical system with only a few degrees of freedom, $H_{\rm bath}$ represents the bath, and $H_{\rm int}$ is the interaction between the two.
We next consider explicit examples and introduce the linear-chain form of quantum impurity models, which is the starting point for an NRG treatment.

Anderson impurity model

The prototype model for strongly correlated systems is the single-band non-degenerate Anderson model [18, 19],

$$H_{AM} = \underbrace{\sum_{\sigma} \varepsilon_d \, n_{d\sigma} + U \, n_{d\uparrow} n_{d\downarrow}}_{H_{\rm imp}} + \underbrace{\sum_{k\sigma} V_{kd} (c^\dagger_{k\sigma} d_\sigma + d^\dagger_\sigma c_{k\sigma})}_{H_{\rm int}} + \underbrace{\sum_{k\sigma} \epsilon_k \, c^\dagger_{k\sigma} c_{k\sigma}}_{H_{\rm bath}} . \tag{3}$$

The first two terms describe the impurity, represented here by a non-degenerate s-level of energy ε_d (see Sec. 6 for generalizations). Electrons in the local level are subject to a Coulomb repulsion U that acts between spin-up and spin-down electrons. The local level hybridizes with the Bloch states of a non-interacting s-wave conduction band, the last term in H_{AM}, with amplitude $V_{\mathbf{k}d}$. The properties of the model are determined by the hybridization function

$$\Delta(\omega) = \pi \sum_k |V_{kd}|^2 \delta(\omega - \varepsilon_k), \tag{4}$$

which, like the conduction density of states $\rho(\omega) = \sum_k \delta(\omega - \varepsilon_k)$, will in general be a complicated function of energy. In cases where the interest is in the very low-energy physics, it is a good approximation to set $\Delta(\omega) \approx \Delta(\varepsilon_F) \equiv \Delta$. In applications to pseudogap systems [20, 21] or to effective quantum impurities in dynamical mean-field theory, the full frequency dependence has to be retained. In applications to quantum dots, the impurity is attached to two baths, the left and right leads, as shown in Fig. 2.[1]

[1] Although such dots are attached to two baths (the left and right leads), for a single level on the dot, only the even combination of left and right lead states couples to the dot. When several levels on the dot are active in transport, one will have a two-channel multi-orbital Anderson model with intra- and inter-orbital Coulomb interactions playing a role (e.g. Hund's exchange).

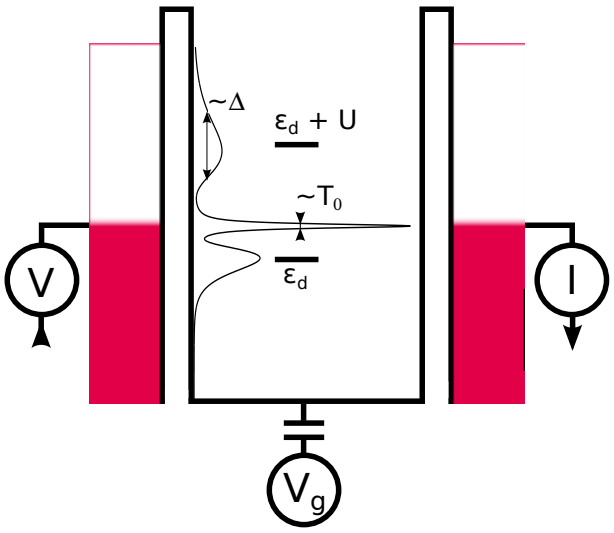

Fig. 2: *A quantum dot with charging energy $U \gg \Delta$ and level energy ε_d connected to left/right leads $H_{\alpha=L/R} = \sum_k \epsilon_{k\alpha\sigma} c^\dagger_{k\alpha\sigma} c_{k\alpha\sigma}$ via tunnel barriers. The gate voltage $V_g \sim \varepsilon_d$ allows changing ε_d relative to ϵ_F and thereby the dot occupation n_d from $n_d = 1$ for $\varepsilon_d = -U/2$ (Kondo regime) to $n_d = 0$ through a mixed valence regime with $n_d \approx 0.5$ for $\varepsilon_d \approx 0$. [22, 23]*

Kondo impurity model

Closely related to the Anderson model, is the Kondo model, which was briefly mentioned in the introduction. We write its Hamiltonian as

$$H_{KM} = \underbrace{-g\mu_B B S_z}_{H_{\rm imp}} + \underbrace{J\vec{S}\cdot\vec{s}_0}_{H_{\rm int}} + \underbrace{\sum_{k\sigma} \varepsilon_k c^\dagger_{k\sigma} c_{k\sigma}}_{H_{\rm bath}}, \tag{5}$$

where we included a magnetic field term $H_{\rm imp} = -g\mu_B B S_z$ to indicate the impurity spin $\vec{S}$ (taken here to be $S = 1/2$ for simplicity), which interacts via an exchange interaction of strength J with the conduction electron spin-density $\vec{s}_0 = \sum_{\sigma\sigma'} f^\dagger_{0\sigma} \vec{\sigma}_{\sigma\sigma'} f_{0\sigma'}$ at the impurity site, where $f_{0\sigma} = \sum_k c_{k\sigma}$ is the local Wannier state of the conduction electrons at the impurity site. The connection to the Anderson model can be established formally via a Schrieffer-Wolff transformation. In essence, provided $\varepsilon_d < 0$ and $\varepsilon_d + U > 0$ so that a single electron occupies the local level in the Anderson model, the physics of both models will be the same at low temperatures.[2] In this case, one finds the correspondence $J = 2V^2(1/(U+\varepsilon_d) - 1/\varepsilon_d)$, which reduces to $8V^2/U$ for the symmetric case $\varepsilon_d = -U/2$ (see discussion of zero bandwidth limit below).

Linear chain representation

For a numerical treatment of the Anderson and Kondo models, it is useful to reformulate them in the form of linear chain models [2,3]. This will allow them to be iteratively diagonalized by a procedure to be described in Sec. 3. We carry this out for the Anderson model: First notice that the impurity state in the Anderson model hybridizes with a local Wannier state $|0\sigma\rangle = f^\dagger_{0\sigma}|{\rm vac}\rangle$,

[2] Strictly speaking, one should also include a potential scattering term in the Kondo model, of the form $\sum_{kk'\sigma} V^{\rm pot}_{kk'} c^\dagger_{k\sigma} c_{k'\sigma}$ for this to be true.

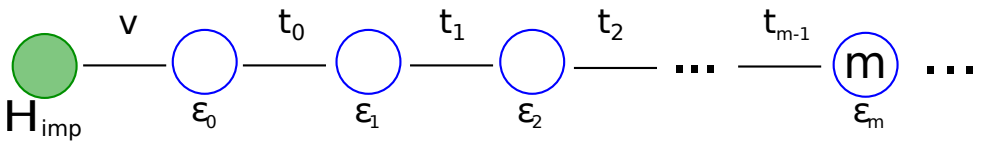

Fig. 3: *The linear-chain form of the Anderson model (9).* $H_{\rm imp} = \varepsilon_d\, n_d + U\, n_{d\uparrow} n_{d\downarrow}$. *The site energies* ε_n *and hoppings* t_n *follow from* $\Delta(\omega)$.

with $|\mathrm{vac}\rangle$ the vacuum state, and $f^\dagger_{0\sigma}$ given by

$$V f^\dagger_{0\sigma} = \sum_k V_{kd} c^\dagger_{k\sigma}. \tag{6}$$

The value of V follows from the normalization $\{f_{0\sigma}, f^\dagger_{0\sigma}\} = 1$

$$V = \left(\sum_k |V_{kd}|^2 \right)^{1/2}. \tag{7}$$

Using the above local state, one can apply the Lanczos procedure (Appendix B) for tridiagonalizing a Hermitian operator, such as $H_{\rm bath}$, to obtain

$$H_{\rm bath} = \sum_{k\sigma} \varepsilon_k\, c^\dagger_{k\sigma} c_{k\sigma} \;\rightarrow\; \sum_{\sigma,n=0}^{\infty} \left[\epsilon_n\, f^\dagger_{n\sigma} f_{n\sigma} + t_n (f^\dagger_{n\sigma} f_{n+1\sigma} + H.c.) \right] \tag{8}$$

with site energies ϵ_n and hoppings t_n depending only on the dispersion ε_k and hybridization V_{kd} through the hybridization function $\Delta(\omega)$, resulting in the linear chain form [2]

$$H_{AM} = \varepsilon_d\, n_d + U\, n_{d\uparrow} n_{d\downarrow} + V \sum_\sigma \left(f^\dagger_{0\sigma} d_\sigma + d^\dagger_\sigma f_{0\sigma} \right) + \sum_{\sigma,n=0}^{\infty} \left[\epsilon_n\, f^\dagger_{n\sigma} f_{n\sigma} + t_n (f^\dagger_{n\sigma} f_{n+1\sigma} + f^\dagger_{n+1\sigma} f_{n\sigma}) \right] \tag{9}$$

depicted in Fig. 3 (with $n_d \equiv \sum_\sigma n_{d\sigma}$). Although formally this model looks like the one-dimensional real-space models treated by the DMRG method [24, 25], the interpretation here is not in terms of electrons hopping on a one-dimensional lattice in real-space. Instead, as will become clearer in Sec. 3, each successive site added along the chain corresponds to adding lower-energy degrees of freedom, measured relative to the Fermi level. By considering longer chains one can then access lower energies.

The same procedure can be used to reformulate any quantum impurity model in terms of an impurity site with local interactions attached to a one-dimensional chain of non-interacting sites. For example, the Kondo model (5) can be rewritten as

$$H_{KM} = -g\mu_B S_z + J \vec{S} \cdot \vec{s}_0 + \sum_{\sigma,n=0}^{\infty} \left[\epsilon_n f^\dagger_{n\sigma} f_{n\sigma} + t_n (f^\dagger_{n\sigma} f_{n+1\sigma} + f^\dagger_{n+1\sigma} f_{n\sigma}) \right]. \tag{10}$$

Zeroth-order approximation for Anderson/Kondo models

A zeroth-order (high energy) approximation to the spectrum of the Anderson model can be obtained by considering just the coupling of the $n = 0$ Wannier state to the impurity and neglecting all others (the zero-bandwidth limit),

$$H_{AM} \approx H_0 \equiv \varepsilon_d \, n_d + U \, n_{d\uparrow} n_{d\downarrow} + V \sum_\sigma \left(f^\dagger_{0\sigma} d_\sigma + d^\dagger_\sigma f_{0\sigma} \right). \tag{11}$$

There are 16 many-electron states $|n_d, n_0\rangle$, which can be classified by the conserved quantum numbers of total electron number N_{el}, total z-component of spin S^{tot}_z and total spin $\vec{S}$. Using these symmetries we can diagonalize the block matrices $H^0_{N_e,S,S_z}$ to obtain the many-body eigenstates $|N_{el}, S, S_z, r\rangle$ and the corresponding eigenvalues. For example, in the product basis $|n_d\rangle|n_0\rangle$, the Hamiltonian for $N_e = 1, S = 1/2, S_z = \pm 1/2$ is given by

$$H_{N_e=1,S=1/2,S_z=\pm 1/2} = \begin{pmatrix} \varepsilon_d & V \\ V & 0 \end{pmatrix}$$

with eigenvalues

$$E_\pm = \left(\varepsilon_d \pm \sqrt{\varepsilon_d^2 + 4V^2} \right) /2 \, .$$

Proceeding similarly for the other Hilbert spaces (exercise), we find that for the particle-hole symmetric case $\varepsilon_d = -U/2$ in the strong correlation limit $U \gg V^2$, the spectrum separates into two groups of states, one group of low-energy states lying close to the (singlet) ground state with spacings $\mathcal{O}(V^2/U)$ and one group of high-energy states lying at energies $\mathcal{O}(U/2)$ higher and also split by $\mathcal{O}(V^2/U)$. This limit corresponds to a singly occupied impurity level effectively behaving as $S = 1/2$. In fact, the 8 lowest states correspond to those obtained from a zeroth-order approximation to the spectrum of the Kondo model via

$$H_{KM} \approx H_0 \equiv J \, \vec{S} \cdot \vec{s}_0 = \frac{J}{2} \left[(\vec{S} + \vec{s}_0)^2 - \vec{S}^2 - \vec{s}_0^2 \right]. \tag{12}$$

The Kondo model is therefore the low-energy effective model of the Anderson model in the limit of strong correlations and single occupancy. By comparing the splitting of the two lowest levels in the Kondo model, the singlet and triplet states, with the corresponding splitting of the same levels in the Anderson model one finds the relation between the bare parameters of the models to be $J = 8V^2/U$, in agreement with the value obtained from the Schrieffer-Wolff transformation $J = 2V^2(1/(U + \varepsilon_d) - 1/\varepsilon_d)$ upon setting $\varepsilon_d = -U/2$ [26].

Within the above zeroth-order approximation, $H \approx H_0$, of the Kondo (and Anderson) model, excitations are unrenormalized. The singlet-triplet excitation (splitting) takes the bare value J. The key ingredient of Wilson's NRG, to be discussed in the next section, is a *controlled procedure* for adding the remaining states $n = 1, 2, \ldots$ neglected in the above zero bandwidth approximation. As we shall see in the calculation of dynamical quantities below, this leads to a drastic renormalization of the spin and single-particle excitations, such that the relevant excitations of the Kondo model are not on the bare scale J but on the Kondo scale

$T_{\rm K} = D(\rho J)^{1/2}\exp(-1/\rho J)$, where $\rho = 1/2D$ is the density of conduction states. One can interpret this large renormalization $J \to T_{\rm K}$ as a renormalization of a bare tunneling amplitude ($J_\perp = J$) due to the dissipative effects of the bath of conduction electrons by a mapping of the (anisotropic) Kondo model onto the dissipative two-state system (also called the spin-boson model). We introduce this and its fermionic equivalents in the next subsection, partly to make the above connection and partly to show that the linear chain representation, which is the starting point for NRG calculations, applies also to bosonic quantum impurity models. For a detailed discussion of the bosonic models within NRG, we refer the reader to the lecture by K. Ingersent.

Spin-boson model and fermionic equivalents

The Hamiltonian of the spin-boson model (SBM) is given by,

$$H_{\rm SB} = \underbrace{-\frac{1}{2}\Delta_0\sigma_x + \frac{1}{2}\epsilon\sigma_z}_{H_{\rm imp}} + \underbrace{\frac{1}{2}\sigma_z\sum_i \lambda_i\left(a_i + a_i^\dagger\right)}_{H_{\rm int}} + \underbrace{\sum_i \omega_i\left(a_i^\dagger a_i + 1/2\right)}_{H_{\rm bath}}. \qquad (13)$$

The first term $H_{\rm imp}$ describes a two-level system with bias splitting ϵ and bare tunneling amplitude Δ_0. The $\sigma_{i=x,y,z}$ are the Pauli spin matrices. The third term, $H_{\rm bath}$, is the environment and consists of an infinite set of harmonic oscillators ($i = 1, 2, \ldots, \infty$) with $a_i(a_i^\dagger)$ the annihilation (creation) operators for a harmonic oscillator of frequency ω_i and $0 \le \omega_i \le \omega_{\rm c}$, where $\omega_{\rm c}$ is an upper cut-off frequency. The non-interacting density of states of the environment is denoted by $g(\omega) = \sum_i \delta(\omega - \omega_i)$ and is finite in the interval $[0, \omega_{\rm c}]$ and zero otherwise. Finally, $H_{\rm int} = \frac{1}{2}\sigma_z\sum_i \lambda_i(a_i + a_i^\dagger)$ describes the coupling of the two-state system coordinate σ_z to the oscillators, with λ_i denoting the coupling strength to oscillator i. The function $\Gamma(\omega + i\delta) = \sum_i(\lambda_i/2)^2/(\omega - \omega_i + i\delta) = \int d\omega'\,(\lambda(\omega')/2)^2\,g(\omega')/(\omega - \omega' + i\delta)$ characterizes the system-environment interaction. For a numerical treatment using the NRG, one proceeds to re-formulate the model (13) in a linear chain form as in (9) and (10) for the Anderson and Kondo models. Thus, one uses the Lanczos procedure and applies $H_{\rm bath}$ repeatedly on the local bosonic orbital $\lambda\, b_0 = \sum_i \lambda_i\, a_i$ to tridiagonalize $H_{\rm bath}$. The resulting linear chain model

$$H_{\rm SB} = \underbrace{-\frac{1}{2}\Delta_0\sigma_x + \frac{1}{2}\epsilon\sigma_z}_{H_{\rm imp}} + \underbrace{\frac{1}{2}\sigma_z\lambda\left(b_0 + b_0^\dagger\right)}_{H_{\rm int}} + \underbrace{\sum_{m=0}^{\infty}\epsilon_m\, b_m^\dagger b_m + t_m\left(b_m^\dagger b_{m+1} + b_{m+1}^\dagger b_m\right)}_{H_{\rm bath}} \qquad (14)$$

may then be treated within NRG in a similar way to the treatment of the Anderson and Kondo models [27], see the lecture by K. Ingersent for details. One difference is that the number of bosons in the eigenstates of $H_{\rm SB}$ is arbitrary, requiring an additional approximation even at the first iteration for $H_0 = H_{\rm imp} + \frac{1}{2}\sigma_z\lambda(b_0 + b_0^\dagger)$ to restrict the maximum number of bosons to a finite number n_b (typically $8 - 10$).

Anisotropic Kondo model

It may be shown via bosonization [28] that the ohmic two-state system, specified by Eq. (13) with a spectral function $J(\omega) = -\frac{1}{\pi}\mathrm{Im}\Gamma(\omega+i\delta) \sim \alpha\,\omega$ for $\omega \to 0$, where α is the dimensionless dissipation strength, is equivalent to the anisotropic Kondo model

$$H_{\mathrm{AKM}} = \underbrace{\frac{J_\perp}{2}(S^+ s_0^- + S^- s_0^+) - g\mu_B B S_z}_{H_{\mathrm{imp}}} + \underbrace{J_\parallel S_z s_0^z}_{H_{\mathrm{int}}} + \underbrace{\sum_{k\sigma} \epsilon_k\, c_{k\sigma}^\dagger c_{k\sigma}}_{H_{\mathrm{bath}}}, \tag{15}$$

where $J_\perp(J_\parallel)$ is the transverse (longitudinal) part of the Kondo exchange interaction and B is a local magnetic field. The correspondence is given by $\rho J_\perp = -\Delta_0/\omega_{\mathrm{c}}$, $-g\mu_{\mathrm{B}}B = \epsilon$, and $\alpha = (1+2\delta/\pi)^2$ where $\delta = \arctan(-\pi\rho J_\parallel/4)$ and $\rho = 1/\omega_c$ is the density of states of the conduction electrons in the anisotropic Kondo model [29–31, 14, 15]. The natural low-energy scale of the ohmic two-state system is the renormalized tunneling amplitude $\Delta_{\mathrm{r}}/\omega_{\mathrm{c}} \approx (\Delta_0/\omega_{\mathrm{c}})^{1/(1-\alpha)}$. A more precise estimate is $\Delta_r/\omega_c = [\sqrt{\Gamma(1-2\alpha)\cos(\pi\alpha)}\,\Delta_0/\omega_c]^{1/(1-\alpha)}$, yielding the known limits $\Delta_r(\alpha \to 0) = \Delta_0$ and $\Delta_r(\alpha \to 1/2) = \frac{\pi}{2}(\Delta_0/\omega_c)^2\,\omega_c$ [15]. For $\alpha > 1/2$, further corrections are needed [15, 32]. It is related to the low-energy Kondo scale T_{K} of the Anisotropic Kondo model. The connection between the (anisotropic) Kondo and ohmic two-state system provides another viewpoint on the local dynamics of a Kondo spin in terms of tunneling and dissipation: The two levels concerned are the two lowest $S_z = 0$ states of H_{imp}, i.e., $|\pm\rangle = 1/\sqrt{2}(|\uparrow\rangle|\downarrow\rangle \pm |\downarrow\rangle|\uparrow\rangle)$ which are connected by $J_\perp$ and tunnel-split by $\Delta_0 = J_\perp$ when $J_\parallel = +\infty$, corresponding to $\alpha = 0$ (decoupled two-level system). A finite $J_\parallel < +\infty$, resulting in a finite $\alpha > 0$, couples these states to the environment and leads to a renormalization of the bare tunneling amplitude $\Delta_0 = J_\perp \to \Delta_r = T_{\mathrm{K}}$, which is particularly drastic in the limit of strong dissipation $\alpha \to 1^-$. Indeed, for $\alpha > 1$, the above correspondence states that $J_\parallel < 0$, which corresponds to the ferromagnetic sector of the Kondo model (see the lecture by A. Nevidomskyy). Since in this limit, $J_\perp$ is irrelevant [19, 26], it follows that T_{K} and hence Δ_r vanish for $\alpha > 1$, i.e., the frictional effects of the environment are so large for $\alpha > 1$ that quantum mechanical tunneling is destroyed at $T = 0$ and tunneling between the two states is possible only via thermal activation. Of interest also is the transition from quantum coherent dynamics at weak dissipation $\alpha \ll 1$ to incoherent dynamics at strong dissipation $\alpha \to 1^-$, see the time-dependent NRG section.

Interacting resonant level model

Finally, the ohmic spin-boson model (SBM) is equivalent to an even simpler fermionic model, the so-called interacting resonant level model (IRLM),

$$H_{\mathrm{IRLM}} = \underbrace{\varepsilon_d\, n_d + V\left(f_0^\dagger d + d^\dagger f_0\right)}_{H_{\mathrm{imp}}} + \underbrace{U_{dc}(n_d - 1/2)(n_0 - 1/2)}_{H_{\mathrm{int}}} + \underbrace{\sum_k \epsilon_k\, c_k^\dagger c_k}_{H_{\mathrm{bath}}}. \tag{16}$$

This model describes a spinless resonant level with energy ε_d hybridizing with a spinless bath of electrons (where we wrote $f_0 = \sum_k c_k$ and $n_0 = f_0^\dagger f_0$) and interacting with the latter via a

non-local Coulomb interaction U_{dc}. Denoting by $\Gamma = \pi\rho V^2$ the width of the resonant level at $U_{dc} = 0$, the correspondence of the SBM to this model is given by $\Delta_0 = 2V \sim \Gamma^{1/2}$, $\varepsilon_d = \epsilon/2$, and $\alpha = (1 + 2\delta/\pi)^2/2$ where $\delta = \arctan(-\pi\rho U_{dc}/2)$. The equivalence between the models can be shown via bosonization and is valid for all $-\infty \leq U_{dc} \leq +\infty$ (describing the sector $2 \geq \alpha \geq 0$) with $U_{dc} = 0$ corresponding to $\alpha = 1/2$ in the SBM. This point marks the crossover from quantum coherent oscillations of the two-level system at $\alpha < 1/2$ to incoherent dynamics at $\alpha > 1/2$, e.g., in the quantity $P(t > 0) \equiv \langle\sigma_z(t)\rangle$ subject to an initial state preparation $\sigma_z = +1$. The physics here is again that of a two-level system (consisting of the single-electron states $|\pm\rangle = (|1\rangle_d|0\rangle_0 \pm |0\rangle_d|1\rangle_0)/\sqrt{2}$ of $H_{\rm imp}$) tunnel-coupled by $\Delta_0 = \sqrt{\varepsilon_d^2 + 4V^2}$. Note that the non-interacting limit $\alpha = 0$ describing the isolated two level system $H_{\rm imp}$ corresponds to $U_{dc} = +\infty$. Strong dissipation ($\alpha > 1/2$) in this model, corresponds to negative U_{dc} and the quantum critical point $\alpha = 1$ occurs at $U_{dc}^* = -(2/\pi\rho)\tan[\pi(\sqrt{2} - 1)/2] \approx -0.969$. For $U_{dc} < U_{dc}^*$ and $\alpha > 1$, quantum mechanical tunneling is absent ($\Delta_r = 0$), and only tunneling via thermal activation is possible (i.e. at $T > 0$). The IRLM is interesting since it is the simplest model that can capture a part of the Kondo physics contained in the Anderson and Kondo models, in particular, the thermodynamic properties and the spin dynamics of the latter: To capture the spin dynamics of the latter within the IRLM, one notes that under the equivalence $S_z \to n_d - 1/2$ the dynamic spin susceptibility of the AKM $\chi_{zz}(\omega) = \langle\langle S_z; S_z\rangle\rangle$ corresponds to the dynamic charge susceptibility $\chi_{dd}(\omega) = \langle\langle n_d; n_d\rangle\rangle$ of the IRLM. Since the IRLM is a spinless model, it is simpler to deal with than the Anderson and Kondo models and we shall use it to illustrate much of the NRG in the next section.

3 Wilson's Numerical Renormalization Group method

Wilson's formulation of the RG for the Kondo model is similar in spirit to Anderson's scaling approach (see Hewson's book [26], Ref. [19] or Nevidomskyy's lecture). The main difference lies in the non-perturbative construction of the RG transformation using a numerical representation of the effective Hamiltonians. The scaling approach uses perturbation theory in the initially small dimensionless coupling (J/D in the Kondo model, or V in the Anderson and IRLM models) to construct such a transformation, but since J/D increases with decreasing energy scale, this approach eventually becomes inaccurate. In the Wilson approach, the RG transformation is perturbative only via a small parameter $\Lambda^{-1/2} < 1$, which is related to the momentum rescaling factor $\Lambda > 1$. The accuracy of the transformation is the same at each step and is independent of the size of the running couplings. For this reason, it gave the first correct description of the crossover from the weak-coupling to the strong-coupling regime of the Kondo model. The NRG procedure involves three steps, illustrated schematically in Fig. 4a-c.

Separation of scales and logarithmic discretization approximation

In quantum impurity problems, the behavior of the system typically changes qualitatively over many energy scales as it passes through a crossover between fixed points. In order to describe

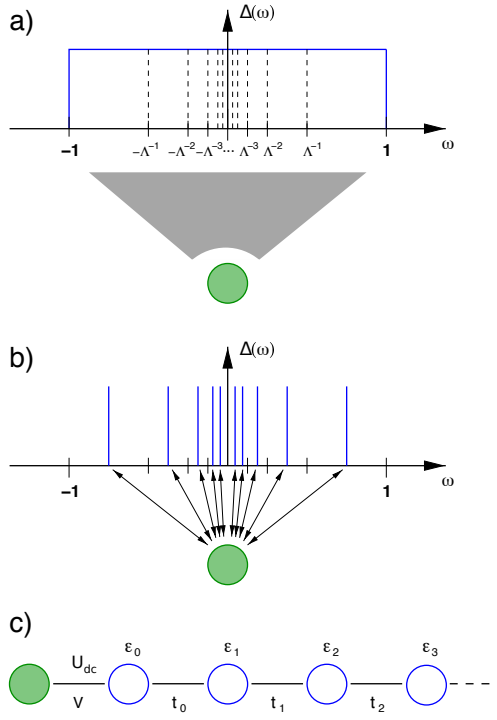

Fig. 4: *Steps in the NRG procedure for a quantum impurity model, here shown for the IRLM. The level (filled circle) hybridizes with strength V to a continuum of conduction states and interacts with these via the Coulomb term U_{dc} ($\Delta(\omega) = \pi\rho V^2$ is here constant). (a) Logarithmic discretization of the continuum conduction band about the Fermi level $\epsilon_F = 0$ into discrete intervals $D_n^+ = [\Lambda^{-(n+1)}, \Lambda^{-n}]$ and $D_n^- = [-\Lambda^{-n}, -\Lambda^{-(n+1)}]$, $n = 0, 1, \ldots$. (b) Within each discrete interval, choose the conduction state most localized on the impurity. (c) Transform this discretized model to linear-chain form, with hoppings now decreasing along the chain and iteratively diagonalize.*

this crossover quantitatively the idea is to separate out the many energy scales in the problem, which arise from the conduction band $[-D, +D]$, and to set up a procedure for treating each scale in turn. We saw in the previous section that it is always possible to rewrite a quantum impurity model in the form of a (semi-infinite) linear chain, see Fig. 3. Truncating this chain to include orbitals $n = 0, \ldots, m$, we have for the IRLM

$$\begin{aligned} H_{\rm IRLM} \approx H_m &= \varepsilon_d\, n_d + V\left(f_0^\dagger d + d^\dagger f_0\right) + U_{dc}(n_d - 1/2)(n_0 - 1/2) \\ &+ \sum_{n=0}^{m} \epsilon_n\, f_n^\dagger f_n + \sum_{n=0}^{m-1} t_n \left(f_n^\dagger f_{n+1} + f_{n+1}^\dagger f_n\right) \end{aligned} \tag{17}$$

with the truncated Hamiltonians H_m satisfying the recursion relation

$$H_{m+1} = H_m + \epsilon_m f_m^\dagger f_m + t_m \left(f_m^\dagger f_{m+1} + f_{m+1}^\dagger f_m\right). \tag{18}$$

Hence, it appears that with this recursion relation, one can iteratively diagonalize the IRLM (and indeed any other QIM) starting from H_0. For the IRLM, H_0 has four eigenstates classified into three Hilbert spaces by the total electron number $N_e = 0, 1, 2$, a conserved quantity (work them out in the product basis $|n_d\rangle|n_0\rangle$). The two one-electron states form the two-level system and are split by the tunnel splitting $\Delta_0 = \sqrt{\varepsilon_d^2 + 4V^2}$. At some point, for sufficiently large m, we will only be able to retain the lowest many-body states of H_m since the Hilbert space grows as $2 \times 2^{m+1}$. The validity of this procedure then depends on whether the perturbation in Eq. (18), the last term involving t_m, is small, once we start neglecting some higher-energy states.[3] In practice, for a quasi-continuous band $H_{\rm bath} = \sum_k \epsilon_k\, c_k^\dagger c_k = \int_{-D}^{+D} d\epsilon\, \epsilon\, c_\epsilon^\dagger c_\epsilon$ the hoppings t_m do

[3] If we keep extending the system by one orbital at a time without neglecting any states, no error is made. The onsite term in ϵ_m is diagonal and shifts the low-energy levels of H_m.

not decay with increasing m, and the above procedure breaks down after some iterations. For example, it can be easily shown for a semi-elliptic density of states $\rho(\epsilon) = \frac{2}{\pi D^2}\sqrt{D^2-\epsilon^2}$, that $t_m = D/2$ for all m (see Hewson's book [26]).

In order to have a working procedure involving decreasing hoppings t_m along the chain, and at the same time achieve the energy scale separation described above, Wilson discretized the conduction band into positive and negative energy intervals, $D_n^+ = [\Lambda^{-(n+1)}, \Lambda^{-n}]$ and $D_n^- = [-\Lambda^{-n}, -\Lambda^{-(n+1)}]$, $n = 0, 1, \ldots$, about the Fermi level $\epsilon_F = 0$ as shown in Fig. 4a.

The quasi-continuous band is then approximated by a discrete one by keeping only a single conduction state from each interval $D_n^{\pm}$,

$$H_{\rm bath} = \int_{-D}^{+D} d\epsilon\, \epsilon\, c_\epsilon^\dagger c_\epsilon \approx \sum_{n=0}^{\infty} \left(\varepsilon_{-n}\, c_{-n}^\dagger c_{-n} + \varepsilon_{+n}\, c_{+n}^\dagger c_{+n} \right) \tag{19}$$

with

$$\varepsilon_{\pm n} = \pm\frac{1}{2} D \left(\Lambda^{-n} + \Lambda^{-(n+1)} \right) = \pm\frac{1}{2} D \Lambda^{-n} \left(1 + \Lambda^{-1} \right). \tag{20}$$

The states $c_{\pm n}^\dagger |vac\rangle$ appearing above are the states in each interval $D_{-n}^{\pm}$ which are most localized near the impurity [2], while the neglected states being orthogonal to these have their wavefunctions localized away from the impurity and are consequently less important (for a more detailed derivation and justification of the logarithmic discretization approximation see Appendix A). By formulating the IRLM as a linear chain using the above logarithmically discretized conduction band, we obtain the same equations (17-18) as above, but, crucially, with hopping parameters t_m (and onsite energies ϵ_m) that now decay exponentially along the chain. For example, for a constant density of states $\rho(\omega) = 1/2D$ and constant hybridization function $\Delta(\omega) = \pi\rho(\omega)V^2 = \Delta_0$ and $\epsilon_F = 0$ one finds for $m = 0, 1, \ldots$ [1]

$$\epsilon_m = 0, \tag{21}$$

$$t_m = \frac{1}{2} D \left(1 + \Lambda^{-1} \right) \Lambda^{-m/2} \xi_m, \tag{22}$$

$$\xi_m = \frac{1 - \Lambda^{-m-1}}{\sqrt{(1 - \Lambda^{-2m-1})(1 - \Lambda^{-2m-3})}}. \tag{23}$$

The ξ_m converge rapidly to 1 with increasing m and we may write $t_m \approx \frac{1}{2} D(1 + \Lambda^{-1})\Lambda^{-m/2}$, so that the IRLM becomes

$$\begin{aligned} H_{IRLM} = {} & \varepsilon_d\, n_d + V \left(f_0^\dagger d + d^\dagger f_0 \right) + U_{dc}(n_d - 1/2)(n_0 - 1/2) \\ & + \frac{1}{2} D(1 + \Lambda^{-1}) \sum_{n=0}^{\infty} \Lambda^{-n/2} \left(f_n^\dagger f_{n+1} + f_{n+1}^\dagger f_n \right). \end{aligned} \tag{24}$$

This Hamiltonian provides a clear separation of the energy scales $\frac{1}{2}(1+\Lambda^{-1})\Lambda^{-n/2}, n = 1, 2, \ldots$ in H and allows the diagonalization of the Hamiltonian in a sequence of controlled steps, each step corresponding to adding an orbital f_n, which is a relative perturbation of strength $\Lambda^{-1/2} < 1$, thereby ensuring convergence of the method. This procedure is described in the following two subsections, where we henceforth restrict ourselves to a constant hybridization with hoppings $t_m \approx \frac{1}{2} D(1 + \Lambda^{-1})\Lambda^{-m/2}$. The procedure is easily generalized to any hybridization function $\Delta(\omega)$ with hoppings t_m decaying sufficiently fast along the chain.

Renormalization group transformation

A renormalization group transformation relating effective Hamiltonians on successive energy scales $\Lambda^{-n/2}$ and $\Lambda^{-(n+1)/2}$ can be set up as follows. First, $H_{\rm IRLM}$ in (24) is truncated to H_m, whose lowest scale is $D_m = \frac{1}{2}D(1+\Lambda^{-1})\Lambda^{-(m-1)/2}$. In order to look for fixed points, we define rescaled Hamiltonians $\bar{H}_m \equiv H_m/D_m$ such that the lowest energy scale of $\bar{H}_m$ is always of order $\mathcal{O}(1)$:

$$\bar{H}_m = \Lambda^{(m-1)/2}\left[\sum_{n=0}^{m-1}\Lambda^{-n/2}(f_n^\dagger f_{n+1} + f_{n+1}^\dagger f_n) + \tilde{\varepsilon}_d\, n_d + \tilde{V}(f_0^\dagger d + d^\dagger f_0) + \tilde{U}_{dc}\left(n_d - \frac{1}{2}\right)\left(n_0 - \frac{1}{2}\right)\right] \tag{25}$$

$$\tilde{\varepsilon}_d = \frac{\varepsilon_d}{\frac{1}{2}D(1+\Lambda^{-1})}\,, \quad \tilde{V} = \frac{V}{\frac{1}{2}D(1+\Lambda^{-1})}\,, \quad \tilde{U}_{dc} = \frac{U_{dc}}{\frac{1}{2}D(1+\Lambda^{-1})}, \tag{26}$$

from which we can recover H as

$$H = \lim_{m\to\infty}\frac{1}{2}D\left(1+\Lambda^{-1}\right)\Lambda^{-(m-1)/2}\bar{H}_m\,. \tag{27}$$

The sequence of rescaled Hamiltonians $\bar{H}_m$ satisfies the recursion relation

$$\bar{H}_{m+1} = \Lambda^{1/2}\bar{H}_m + \left(f_m^\dagger f_{m+1} + f_{m+1}^\dagger f_m\right) \tag{28}$$

and allows a RG transformation $\mathcal{T}$ to be defined:

$$\bar{H}_{m+1} = \mathcal{T}[\bar{H}_m] \equiv \Lambda^{1/2}\bar{H}_m + \left(f_m^\dagger f_{m+1} + f_{m+1}^\dagger f_m\right) - \bar{E}_{G,m+1} \tag{29}$$

with $\bar{E}_{G,m+1}$ the ground-state energy of $\bar{H}_{m+1}$. In fact $\mathcal{T}$ defined in (29) may not have fixed points since it relates a Hamiltonian with an even number of orbitals to a Hamiltonian with an odd number of orbitals. If this happens, then $\mathcal{R} = \mathcal{T}^2$ can be defined as the RG transformation, and this will have fixed points, a set of even m fixed points and a set of odd m fixed points:

$$\bar{H}_{m+2} = \mathcal{R}[\bar{H}_m] \equiv \mathcal{T}^2[\bar{H}_m]\,. \tag{30}$$

Iterative diagonalization scheme

The transformation R relates effective Hamiltonians $H_m = D_m\bar{H}_m$ and $H_{m+1} = D_{m+1}\bar{H}_{m+1}$ on decreasing scales $D_m > D_{m+1}$. It can be used to iteratively diagonalize the Anderson Hamiltonian by the following sequence of steps:

1. the local part

$$\bar{H}_0 = \Lambda^{-1/2}\left[\tilde{\varepsilon}_d\, n_d + \tilde{V}\left(f_0^\dagger d + d^\dagger f_0\right) + \tilde{U}_{dc}(n_d - 1/2)(n_0 - 1/2)\right], \tag{31}$$

   which contains the many-body interactions, is diagonalized to yield the eigenstates $|q\rangle$ (the "zeroth" order step described above and in Sec. 2),

2. assuming that $\bar{H}_m$ has been diagonalized for some $m \geq 0$,

$$\bar{H}_m = \sum_q \bar{E}_q^m \, |q\rangle\langle q|$$

we add a "site" and use Eq. (29) to set up the matrix for $\bar{H}_{m+1}$ within a product basis $|q, \alpha_{m+1}\rangle = |q\rangle_m |\alpha_{m+1}\rangle$ consisting of the eigenstates $|q\rangle_m$ of $\bar{H}_m$ and the states of the next orbital along the chain $|\alpha_{m+1}\rangle$ ($|0\rangle$ for $\alpha_{m+1} = 1$ and $|1\rangle$ for $\alpha_{m+1} = 2$),

$$\begin{aligned}\langle q, \alpha_{m+1}|\bar{H}_{m+1}|q', \alpha'_{m+1}\rangle &= \Lambda^{1/2}\, \delta_{\alpha_{m+1},\alpha'_{m+1}} \delta_{q,q'}\, \bar{E}_q^m \\ &+ (-1)^{N_{e,q'}}\ {}_m\langle q|f_m^\dagger|q'\rangle_m\ \langle\alpha_{m+1}|f_{m+1}|\alpha'_{m+1}\rangle \\ &+ (-1)^{N_{e,q}}\ \langle\alpha_{m+1}|f_{m+1}^\dagger|\alpha'_{m+1}\rangle_m\ \langle q|f_m|q'\rangle_m\,, \end{aligned} \tag{32}$$

with $N_{e,q}, N_{e,q'}$ the number of electrons in $|q\rangle$ and $|q'\rangle$, respectively. This is diagonalized and the procedure is repeated for the next energy shell as depicted in Fig. 4c. Since $\bar{H}_m$ is already diagonalized, the off-diagonal matrix elements, involving ${}_m\langle q|f_{m\sigma}^\dagger|q'\rangle_m = {}_m\langle q'|f_{m\sigma}|q\rangle_m^\dagger$, can be expressed in terms of the known eigenstates of $\bar{H}_m$ by using the unitary transformation relating product states $|q\rangle_{m-1}|\alpha_m\rangle$ to eigenstates $|q\rangle_m$ of $\bar{H}_m$

$$|q\rangle_m = \sum_{r,\alpha_m} U_m(r\alpha_m, q)|q\rangle_{m-1}|\alpha_m\rangle, \tag{33}$$

where U_m is the matrix of eigenvectors of $\bar{H}_m$.

Equation (33) also shows that the NRG eigenstates have the form of so called matrix product states (MPS) [33], a feature of NRG shared also by the density matrix renormalization group method (DMRG) for one-dimensional quantum systems [24, 25]. In order to see this, we introduce the notation $A^{\alpha_m}_{q_m q_{m-1}} \equiv U_m(q_{m-1}\alpha_m, q_m)$ with $|q_m\rangle \equiv |q\rangle_m$ and repeatedly apply Eq. (33) to obtain

$$\begin{aligned}|q_m\rangle &= \sum_{q_{m-1},\alpha_m} A^{\alpha_m}_{q_{m-1}q_m}|q_{m-1}\rangle|\alpha_m\rangle \\ &= \sum_{q_{m-1},\alpha_m} A^{\alpha_m}_{q_{m-1}q_m}\left[\sum_{q_{m-2}\alpha_{m-1}} A^{\alpha_{m-1}}_{q_{m-2}q_{m-1}}|\alpha_{m-1}\rangle\right]|\alpha_m\rangle \\ &= \sum_{q_{m_0},\alpha_{m_0+1}\ldots\alpha_m} \left(A^{\alpha_{m_0+1}}\ldots A^{\alpha_m}\right)_{q_{m_0}q_m}|\alpha_{m_0+1}\rangle\ldots|\alpha_m\rangle, \end{aligned} \tag{34}$$

where $m_0 \geq 0$.

3. In order to reduce the size of the matrices that need to be diagonalized, one uses available symmetries, such as conservation of total electron number, or in models with spin degrees of freedom with rotational symmetry, conservation of total spin. For multi-channel models, such as the three-channel Kondo model, additional symmetries, such as $SU(3)$, may be used to significantly reduce the numerical effort [34, 35]. The use of symmetries, beyond the advantage of reducing the computational cost, also improves the accuracy of the calculations once one starts to neglect high-energy states (see next subsection), since it avoids the possibility of splitting up degenerate states within a multiplet carrying the same conserved quantum numbers.

Truncation

In practice, since the number of many-body states in $\bar{H}_m$ grows as $2 \times 2^{m+1}$ for the IRLM and as $4 \times 4^{m+1}$ for the Anderson or Kondo models, it is not possible to retain all states after a given iteration $m = m_0$. Keeping 1024 states results in $m_0 = 8$ for the IRLM and $m_0 = 3$ for the Anderson model. We denote the retained states of $\bar{H}_m$ by $|k\rangle_m$, while the higher-energy states neglected are denoted by $|l\rangle_m$, see Fig. 12 in Sec. 5. While only kept states are used to set up and diagonalize the sequence of Hamiltonians $\bar{H}_m, m = m_0, m_0 + 1, ...$ up to a maximum chain size of length $m = N$, we shall see later that the discarded states $|l\rangle_m$ from each iteration $m \geq m_0$ prove to be very useful for calculating physical properties.
The truncation of the spectrum of $\bar{H}_m$ restricts the range of eigenvalues in $H_m = D_m \bar{H}_m$ to be such that $0 \leq E_q^m \leq K D_m$ where $K = K(\Lambda)$ depends on Λ and the number of states retained. For 1000 states and $\Lambda = 3$, $K(\Lambda) \approx 10$. However, eigenvalues below D_m are only approximate eigenvalues of the infinite system H, since states with energies below D_m are calculated more accurately in subsequent iterations $m+1, m+2, \ldots$. Therefore the part of the spectrum of H_m that is close to the spectrum of H is restricted to $D_m \leq E_q^m \leq K(\Lambda) D_m$. This allows the whole spectrum of H to be recovered by considering the spectra of the sequence of Hamiltonians H_m, $m = 0, 1, \ldots$. In this way, the many–body eigenvalues and eigenstates are obtained on all energy scales. Due to the smallness of the perturbation (of $\mathcal{O}(\Lambda^{-1/2}) < 1$) in adding an energy shell to go from H_m to H_{m+1}, the truncation of the high-energy states turns out, in practice, to be a very good approximation.

Fixed points

The analysis of fixed points is important to gain a conceptual understanding of the model and for accurate analytic calculations in the vicinity of a fixed point [2].
From (30), a fixed point H^* of $\mathcal{R} = \mathcal{T}^2$ is defined by

$$H^* = \mathcal{R}[H^*]. \tag{35}$$

Proximity to a fixed point is identified by ranges of m, $m_1 \leq m \leq m_2$, where the energy levels $\bar{E}_p^m$ of $\bar{H}_m$ are approximately independent of m: $\bar{E}_p^m \approx \bar{E}_p$ for $m_1 \leq m \leq m_2$. A typical energy level flow diagram showing regions of m where the energy levels are approximately constant is shown in Fig. 5a for the anisotropic Kondo model (AKM) [30]

$$H_{AKM} = \sum_{k\sigma} \varepsilon_k \, c_{k\sigma}^\dagger c_{k\sigma} + \frac{J_\perp}{2} \left(S^+ f_{0\downarrow}^\dagger f_{0\uparrow} + S^- f_{0\uparrow}^\dagger f_{0\downarrow} \right) + \frac{J_\parallel}{2} S_z \left(f_{0\uparrow}^\dagger f_{0\uparrow} - f_{0\downarrow}^\dagger f_{0\downarrow} \right). \tag{36}$$

There is an unstable high-energy fixed point (small m) and a stable low-energy fixed point (large m). The low-energy spectrum is identical to that of the isotropic Kondo model at the strong-coupling fixed point $J = \infty$ in [1] (e.g. the lowest single-particle excitations in Fig. 5a, $\eta_1 = 0.6555$, $\eta_2 = 1.976$ agree with the $\Lambda = 2$ results of the isotropic model in [1]). The crossover from the high-energy to the low-energy fixed point is associated with the Kondo scale

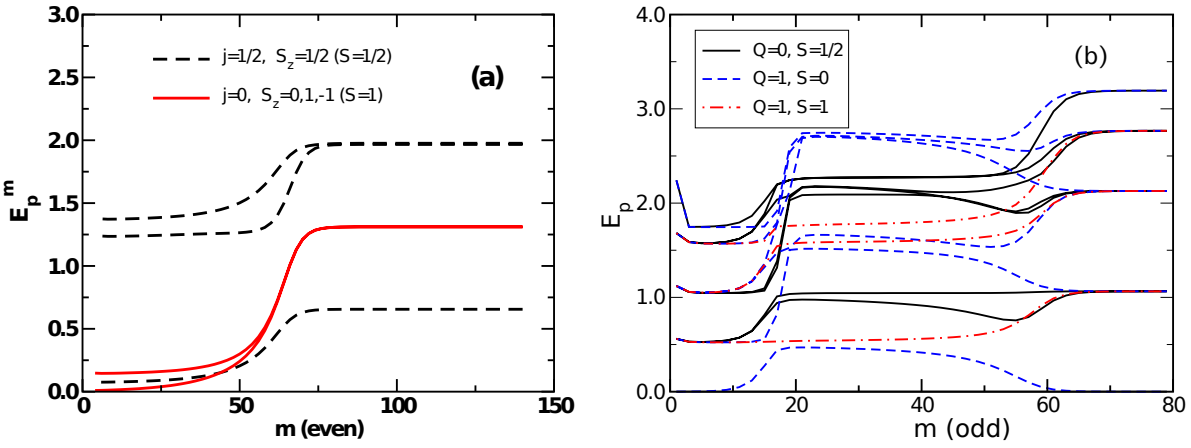

Fig. 5: (**a**) *The lowest rescaled energy levels of the AKM for* $J_{\|} = 0.443$ *and* $J_{\perp} = 0.01$. *The states are labeled by conserved pseudospin* j *and total* S_z *(adapted from [30]).* (**b**) *The flow of the lowest many-body energy levels of the Anderson model for* $\varepsilon_d = -U/2$, $U/\pi\Delta_0 = 12.66$, *and* $\Lambda = 2.5$. *States are labeled by quantum numbers for total charge* Q *and total spin* S *(adapted from [4, 2]).*

$T_{\rm K}$. Spin-rotational invariance, broken at high energies, is restored below this scale (e.g., the $j = 0$ states with $S_z = 0$ and $S_z = \pm 1$ become degenerate below $T_{\rm K}$ and can be classified by the same total spin S as indicated in Fig. 5a). In Fig. 5b typical energy level flows for the symmetric Anderson impurity model $\varepsilon_d = -U/2$ in the strongly correlated Kondo regime are shown. Here, one sees three fixed points: an unstable free orbital fixed point for $m < 10$, a marginal fixed point for $10 < m < 50$ corresponding to formation of a local moment interacting weakly via the antiferromagnetic Kondo exchange with the conduction electrons. In this region, the effective Hamiltonian is essentially the Kondo model. Finally, for $m > 50$ there is a flow to the stable strong-coupling fixed point, characterized by a fixed-point spectrum obtained by setting $J = \infty$, i.e., the local spin and local conduction orbital are frozen out. The fixed-point spectrum is then that of a free electron chain with one site removed, i.e., there is a crossover to an even m fixed-point spectrum. The freezing out of the local spin implies that inelastic scattering processes are blocked as $m \to \infty$ ($T \to 0$), and one obtains the picture of a renormalized Fermi liquid at low temperatures.

Analytic calculations can be carried out in the vicinity of these various fixed points by setting up effective Hamiltonians $H_{\rm eff} = H^* + \sum_\lambda \omega_\lambda O_\lambda$, where the leading deviations O_λ about H^* can be obtained from general symmetry arguments. This allows, for example, thermodynamic properties to be calculated in a restricted range of temperatures, corresponding to the restricted range of m where $\bar{H}_m$ can be described by a simple effective Hamiltonian $H_{\rm eff}$. In this way Wilson could show that the ratio of the impurity susceptibility, $\chi_{\rm imp}$, and the impurity contribution to the linear coefficient of specific heat, $\gamma_{\rm imp}$, at $T = 0$, is twice the value of a non-interacting Fermi liquid: $R = 4\pi^2\chi_{imp}/3\gamma_{imp} = 2$. We refer the reader to the detailed description of such calculations in [1, 2], and we turn now to the numerical procedure for calculating physical properties, which can give results at all temperatures, including the crossover regions.

4 Calculation of physical properties

The ability of the method to yield thermodynamic, dynamic, and transport properties makes it very useful for interpreting experimental results.[4] We shall first describe the calculation of thermodynamics and dynamics using conventional approaches (without use of the complete basis set, but including reduced density matrices for dynamics) [2, 7, 8]. In Sec. 5 we shall then discuss more recent approaches using the complete basis set and full density matrix [12, 10] (this division, however, is somewhat arbitrary).

Thermodynamics: conventional approach

Suppose we have diagonalized exactly the Hamiltonian for a quantum impurity model such as the Kondo model and have all the many-body eigenvalues E_q and eigenstates $|q\rangle$

$$H = \sum_q E_q \, |q\rangle\langle q| \equiv \sum_q E_q \, X_{qq} \, . \tag{37}$$

We can then calculate the partition function

$$Z(T) \equiv \mathrm{Tr}\, e^{-H/k_{\mathrm{B}}T} = \sum_q e^{-E_q/k_{\mathrm{B}}T} \tag{38}$$

and hence the thermodynamics via the impurity contribution to the free energy $F_{\mathrm{imp}}(T) = -k_{\mathrm{B}}T \ln Z/Z_c$, where $Z_c = Tr\ e^{-H_c/k_{\mathrm{B}}T}$ is the partition function for the non-interacting conduction electrons. In the NRG procedure we can only calculate the "shell partition functions" Z_m for the sequence of truncated Hamiltonians H_m

$$Z_m(T) \equiv \mathrm{Tr}\, e^{-H_m/k_{\mathrm{B}}T} = \sum_q e^{-E_q^m/k_{\mathrm{B}}T} = \sum_q e^{-D_m \bar{E}_q^m/k_{\mathrm{B}}T} \, . \tag{39}$$

We will have $Z_m(T) \approx Z(T)$ provided

1. we choose $k_{\mathrm{B}}T = k_{\mathrm{B}}T_m \ll E^m_{max} = D_m K(\Lambda)$ so that the contribution to the partition function from excited states $E_q^m > D_m K(\Lambda)$, not contained in Z_m, is negligible, and

2. the truncation error made in replacing H by H_m in equating (38) and (39) is small. This error has been estimated in [2] to be approximately $\Lambda^{-1} D_m / k_{\mathrm{B}}T_m$.

Combining these two conditions requires that

$$\frac{1}{\Lambda} \ll \frac{k_{\mathrm{B}}T_m}{D_m} \ll K(\Lambda). \tag{40}$$

The choice $k_{\mathrm{B}}T = k_{\mathrm{B}}T_m \approx D_m$ is reasonable and allows the thermodynamics to be calculated at a sequence of decreasing temperatures $k_{\mathrm{B}}T_m \sim D_m, N = 0, 1, \ldots$ from the truncated partition functions Z_m. The procedure yields essentially exact results. For small $\Lambda \lesssim 3$, the window

[4] Spatial correlations may also be investigated, see Ref. [36]

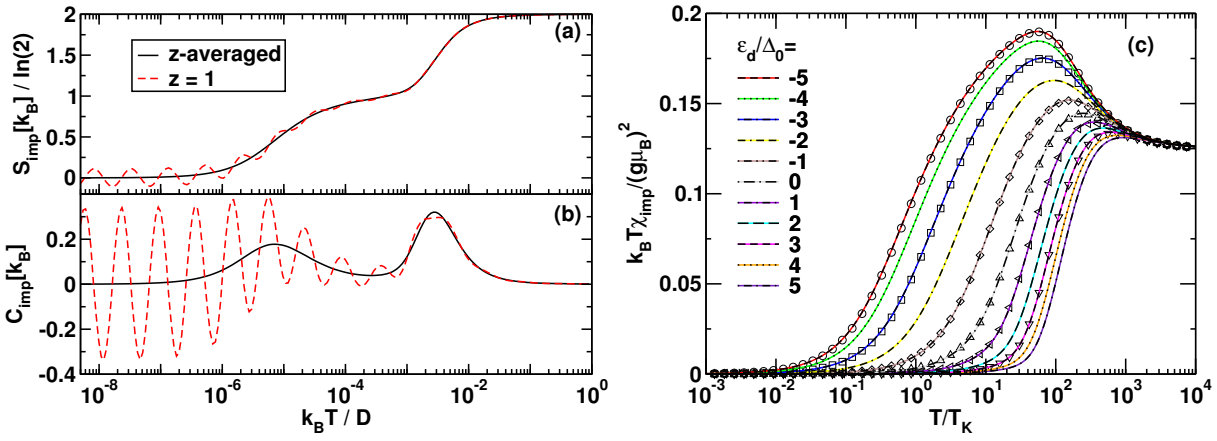

Fig. 6: *Temperature dependence of, (a), the impurity entropy, $S_{\rm imp}(T)$, and, (b), the impurity specific heat, $C_{\rm imp}(T)$, for the symmetric Anderson model with $U/\Delta_0 = 12$ and $\Delta_0 = 0.001D$. The calculations are for $\Lambda = 4$, without z-averaging [$n_z = 1$, $z = 1$ (dashed lines)], and with z-averaging [$n_z = 2$, $z = 1/4, 3/4$ (solid lines)]. For $\Lambda = 4$ two z values suffice to eliminate the discretization oscillations [37]. (c) Impurity susceptibility, $\chi_{\rm imp}(T)$, vs $T/T_{\rm K}$ for the asymmetric Anderson model with the same parameters as above and several values of ε_d/Δ_0 with $T_{\rm K}$ for the symmetric model. Broken lines: FDM approach. Solid lines: conventional approach. Symbols: Bethe ansatz (for selected values of $\varepsilon_d/\Delta_0 = -5, -3, -1, 0, +1, +3$). NRG parameters: $\Lambda = 10$ with z-averaging [$n_z = 4$, $z = 1/8,\ 1/2,\ 3/8,\ 3/4$] [38].*

for choosing the temperature T_m to satisfy Eq. (40) is small, and typically only one such temperature is used for each shell. For larger $\Lambda \gg 1$ one can use many temperatures $T_m^i, i = 1, ..., n_T$ that satisfy the above condition; however, for large $\Lambda = 4 - 10$, discretization oscillations become important [39, 40]. This problem is overcome by averaging the results over several discretizations of the band, i.e., one carries out several calculations with discretizations of the band $\pm D, \pm D\Lambda^{-(1-z_k)}, \pm D\Lambda^{-(2-z_k)}, ...$ and averages the results for several $z_k, k = 1, ..., N_z$. Figures 6a and b illustrate this for the entropy and specific heat of the Anderson model. In this way, the conventional approach can recover essentially exact results for thermodynamics. Fig. 6c shows a comparison for the impurity static spin susceptibility of the Anderson impurity model

$$\chi_{\rm imp}(T) = \frac{(g\mu_B)^2}{k_{\rm B}T}\left[\frac{1}{Z}Tr\ (S_z^{\rm tot})^2 e^{-H/k_{\rm B}T} - \frac{1}{Z_c}Tr\ (S_{z,c}^{\rm tot})^2 e^{-H_c/k_{\rm B}T}\right]$$

to both Bethe-ansatz results and results obtained within the more recent full density matrix approach to be described below.

Figure 7a illustrates the evolution of the impurity specific heat of the IRLM with increasing dissipation strength α: for $\alpha \ll 1$ the specific heat curve fits that of an isolated two-level system $C(T) \sim (T_0/T)^2/\cosh^2(T_0/T)$ except at $T \ll T_0$ where the behavior is linear in T (as expected for any finite α), while for $\alpha \to 1$ the specific heat curves approach the universal Kondo specific heat curve for the isotropic Kondo model. Fig. 7b demonstrates also the very good agreement of the IRLM results with corresponding Bethe Ansatz calculations for the AKM, further illustrating the equivalence of these models for thermodynamic properties.

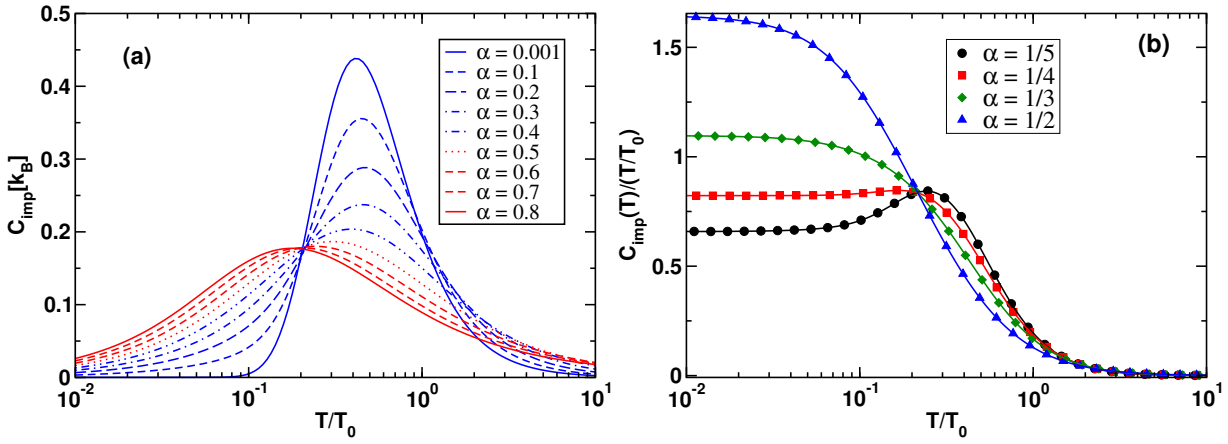

Fig. 7: *(a) Evolution of the impurity specific heat, $C_{\rm imp}(T)$, of the IRLM with increasing dissipation strength α, and, (b), $C_{\rm imp}(T)/(T/T_0)$, for the IRLM at several α (symbols) compared to the corresponding Bethe Ansatz results for the equivalent AKM [31] (lines). The conventional approach was used for the NRG calculations with $\Lambda = 4$ and z-averaging with $n_z = 8$. The low-energy scale T_0 was extracted from the local charge susceptibility of the IRLM and corresponds to the renormalized tunneling amplitude Δ_r of this model, up to factors of order unity.*

Dynamics: conventional approach without reduced density matrices

We consider now the application of the NRG method to the calculation of dynamic properties of quantum impurity models [41,6–8]. For definiteness we consider the Anderson impurity model and illustrate the procedure for the impurity spectral density $A_{d\sigma}(\omega,T) = -\frac{1}{\pi}\mathrm{Im}\, G_{d\sigma}(\omega,T)$ with

$$G_{d\sigma}(\omega,T) = \int_{-\infty}^{+\infty} d(t-t')\, e^{i\omega(t-t')} G_{d\sigma}(t-t') \tag{41}$$

$$G_{d\sigma}(t-t') = -i\theta(t-t') \left\langle [d_\sigma(t), d_\sigma^\dagger(t')]_+ \right\rangle_\varrho \tag{42}$$

with the density matrix ϱ of the system.

Suppose we have all the many-body eigenstates $|q\rangle$ and eigenvalues E_q of the Anderson impurity Hamiltonian H. Then the density matrix, $\varrho(T)$, of the full system at temperature $k_{\rm B}T = 1/\beta$ can be written

$$\varrho(T) = \frac{1}{Z(T)} \sum_q e^{-\beta E_q}\, |q\rangle\langle q|\,, \tag{43}$$

the impurity Green function can be written in the Lehmann representation as

$$G_{d\sigma}(\omega,T) = \frac{1}{Z(T)} \sum_{q,q'} |\langle q|d_\sigma|q'\rangle|^2\, \frac{e^{-E_q/k_{\rm B}T} + e^{-E_{q'}/k_{\rm B}T}}{\omega - (E_{q'} - E_q)} \tag{44}$$

and the corresponding impurity spectral density $A_{d\sigma}$ as

$$A_{d\sigma}(\omega,T) = \frac{1}{Z(T)} \sum_{q,q'} |M_{q,q'}|^2 (e^{-E_q/k_{\rm B}T} + e^{-E_{q'}/k_{\rm B}T})\, \delta(\omega - (E_{q'} - E_q)) \tag{45}$$

with $M_{q,q'} = \langle q|d_\mu|q'\rangle$.

Consider first the case $T = 0$ ($T > 0$ is described in the next section), then

$$A_{d\sigma}(\omega, T=0) = \frac{1}{Z(0)} \sum_q |M_{q,0}|^2 \, \delta(\omega + (E_q - E_0)) + \frac{1}{Z(0)} \sum_{q'} |M_{0,q'}|^2 \, \delta(\omega - (E_{q'} - E_0)), \quad (46)$$

with $E_0 = 0$ the ground-state energy. In order to evaluate this from the information which we actually obtain from an iterative diagonalization of H, we consider the impurity spectral densities corresponding to the sequence of Hamiltonians H_m, $m = 0, 1, \ldots, N$,

$$A^m_{d\sigma}(\omega, T=0) = \frac{1}{Z_m(0)} \sum_q |M^m_{q,0}|^2 \, \delta(\omega + E^m_q) + \frac{1}{Z_m(0)} \sum_{q'} |M^m_{0,q'}|^2 \, \delta(\omega - E^m_{q'}) \, . \quad (47)$$

From the discussion on the spectrum of H_m in the previous section, it follows that the ground-state excitations of H_m that are representative of the infinite system H are those in the range $D_m \leq \omega \leq K(\Lambda) D_m$. Lower energy excitations and eigenstates are calculated more accurately at subsequent iterations, and higher energy excitations are not contained in H_m due to the elimination of the higher energy states at each m. Hence, for fixed m, we can approximately evaluate the spectral density at a characteristic frequency $\omega \approx \omega_m \equiv k_{\rm B} T_m$ via

$$A_{d\sigma}(\omega, T=0) \approx A^m_{d\sigma}(\omega, T=0), \quad m = 0, 1, \ldots, N. \quad (48)$$

In making this approximation, we are assuming that the matrix elements $M^m_{0,q'}$ of the finite-system Hamiltonian are the same as those of the infinite system $M_{0,q'}$. This assumption fails when an applied field strongly affects the groundstate and low lying excited states, thereby making also the matrix elements for the finite-size system $M^m_{0,q'}$ appreciably different from those of the infinite system. We shall come back to this point below, when we introduce the reduced density matrix approach to Green functions [8]. Returning to the calculation of spectral densities, a typical choice for the characteristic frequency to evaluate $A_{d\sigma}(\omega, 0)$ from $A^m_{d\sigma}(\omega, 0)$ is $\omega = 2\omega_m$ for $\Lambda = 2$. In this way $A_{d\sigma}(\omega, T = 0)$ can be calculated at a sequence of decreasing frequencies $\omega = 2\omega_m, m = 0, 1, \ldots, N$ from the quantities $A^m_{d\sigma}$. In practice we are not interested in the discrete spectra $A^m_{d\sigma}(\omega) = \sum_q w^m_q \, \delta(\omega - E^m_q)$ of the Hamiltonians H_m but in continuous spectra that can be compared with experiment. Smooth spectra can be obtained from the discrete spectra by replacing the delta functions $\delta(\omega - E^m_q)$ by smooth distributions $P_m(\omega - E^m_q)$. A natural choice for the width η_m of P_m is D_m, the characteristic scale for the energy level structure of H_m. Two commonly used choices for P are the Gaussian and the Logarithmic Gaussian distributions [7,41,42]. More refined schemes also exist [43,44], as well as different band discretizations to reduce artifacts close to band edges [45]. A peak of intrinsic width Γ at frequency Ω_0 will be well resolved by the above procedure provided that $\Omega_0 \ll \Gamma$, which is the case for the Kondo resonance and other low-energy resonances. In the opposite case, the low (logarithmic) resolution at higher frequencies may be insufficient to resolve the intrinsic widths and heights of such peaks. Usually such higher frequency peaks are due to single-particle processes and can be adequately described by other methods (exceptions include interaction dominated features in the ohmic two-state system, see below, and in strongly correlated lattice models in high dimensions [16, 46–48]). In both cases, $\Omega_0 \ll \Gamma$ and $\Omega_0 \gg \Gamma$, the

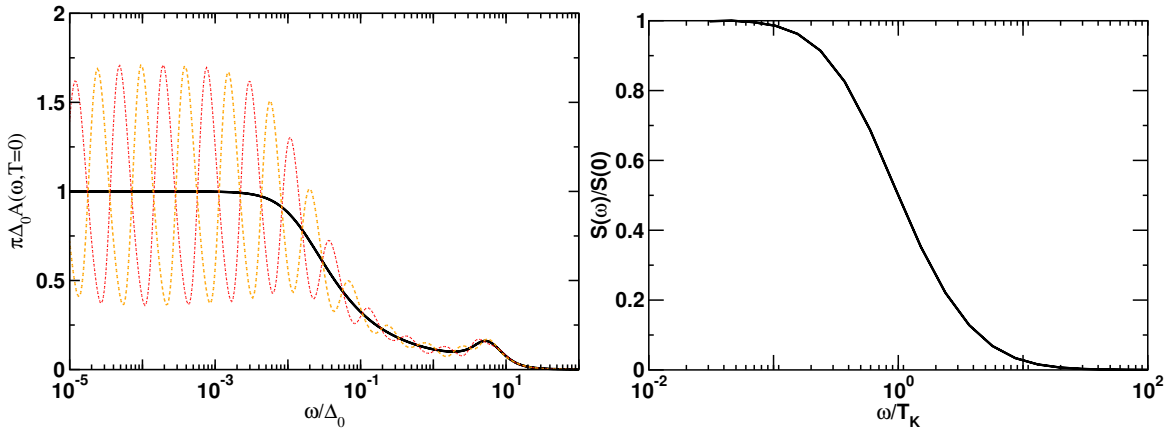

Fig. 8: *(**a**) The impurity spectral density for the symmetric Anderson model for $U/\Delta_0 = 12$ at large $\Lambda = 10$ showing discretization oscillations for two values of z. Averaging over 8 z-values yields the smooth curve. (**b**). Longitudinal spin relaxation function $S(\omega)/S(0)$ versus $\omega/T_{\rm K}$ for the isotropic Kondo model, showing that the spin relaxes incoherently.*

positions and intensities of such peaks are given correctly. An alternative procedure for obtaining smooth spectra, which in principle resolves finite frequency peaks with the same resolution as the low-energy peaks, has been proposed in [49] and uses the averaging over several band discretizations, described above for the thermodynamics. This procedure allows carrying out calculations for spectral functions at larger Λ. An example is shown in Fig. 8a for the symmetric Anderson model. As in the thermodynamics, calculations of the dynamics at large $\Lambda \gg 1$ exhibit discretization oscillations, see Fig. 8a, which may be eliminated by averaging over several band discretizations.

How accurate is the NRG for dynamic properties? A good measure of the accuracy of the procedure is given by the Friedel sum rule, a Fermi liquid relation which states that [26]

$$A_{d\sigma}(0) = \frac{1}{\pi\Delta_0}\sin^2(\pi n_d/2), \qquad n_d = \int_{-\infty}^{0} d\omega\; A_{d\sigma}(\omega)\,. \tag{49}$$

From Fig. 8a we find that $\pi\Delta_0 A_{d\sigma}(0,0) = 1 \pm 10^{-3}$, i.e., the Friedel sum rule is satisfied to within 0.1% relative error. More important, however, is that this error remains small independent of the interaction strength $0 \le U \le \infty$. Two-particle Green functions and response functions, such as the longitudinal dynamical spin susceptibility $\chi_{zz} = \langle\langle S_z; S_z\rangle\rangle$, and the corresponding relaxation function, $S(\omega) = -\frac{1}{\pi}\chi''_{zz}(\omega)/\omega$, of the Anderson impurity model and of the (anisotropic) Kondo model can also be calculated with comparable accuracy to single-particle spectral functions [30]. The spin relaxation function for the Kondo model is shown in Fig. 8b and illustrates the statement made in Sec. 2 that the spin excitations of the Kondo model are drastically renormalized from the bare value of J down to the Kondo scale $T_{\rm K}$ due to the frictional effects of the environment.

The procedure for calculating finite temperature dynamical quantities, like $A_{d\sigma}(\omega, T)$, required as input for calculating transport properties is similar to that for the $T = 0$ dynamics described above [7]. The spectral density $A_{d\sigma}(\omega, T)$ at fixed temperature T is evaluated as above at

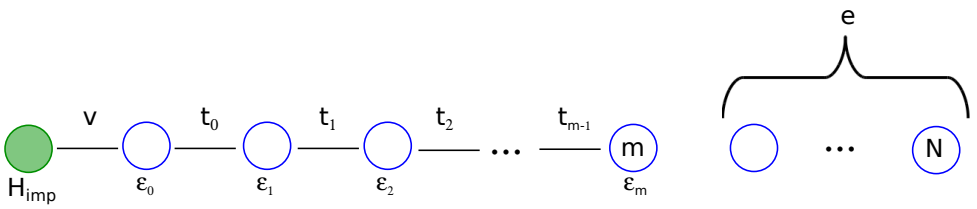

Fig. 9: *The Hilbert space of H_m is supplemented with $N-m$ environment degrees of freedom $e=(\alpha_{m+1},...,\alpha_N)$ [8].*

frequencies $\omega \approx 2\omega_m, m=0,1,\ldots,M \leq N$ until $2\omega_M$ becomes of order $k_{\rm B}T$, i.e., $2\omega_M = \alpha k_{\rm B}T$ with $\alpha \approx 1$. To calculate the spectral density at frequencies $\omega < k_{\rm B}T$ a smaller "cluster" is used. This is done because when $k_{\rm B}T$ is larger than the frequency at which the spectral density is being evaluated, it is the excited states of order $k_{\rm B}T$ contained in previous clusters that are important and not the excitations very much below $k_{\rm B}T$. This approach suffers from the same criticism as the $T=0$ approach above, namely one is using a finite cluster H_m to approximate $M_{q',q} \approx M^m_{q',q}$ (and also $Z(T) \approx Z_m(T)$). In particular, for $\omega < k_{\rm B}T$, the use of a small cluster of size $M < N$ does not capture the full information available, a deficiency that is corrected by the full density matrix approach. Nevertheless, this early approach gives remarkably good results for finite temperature spectra and transport properties [7].

Dynamics: conventional approach with reduced density matrices

A way of reducing finite-size errors, inherent in the above approach to Green functions, has been proposed by Hofstetter [8] and further developed within the full density matrix approach. As mentioned above, there are situations when a small field can strongly polarize the low-energy states of H_m, thereby strongly affecting the matrix elements $M^m_{q',q}$ and hence the spectra. For example, a magnetic field $B \approx T_{\rm K}$ in the Anderson model is sufficiently strong to polarize the groundstate such that $n_{d\uparrow} \approx 1$ and $n_{d\downarrow} \approx 0$ at $T \ll T_{\rm K}$. In this case, the use of the canonical density matrix $\varrho(T) \approx \varrho_m(T) = \frac{1}{Z_m(T)}\sum_q e^{-\beta E^m_q}|q\rangle\langle q|$ in evaluating the spectra on scales $\omega_m \gg T_{\rm K}$ can result in large errors. A solution to this is to use $\varrho_N(T) = \frac{1}{Z_N(T)}\sum_q |q\rangle e^{-\beta E^N_q}\langle q|$ for the longest chain diagonalized and to evaluate the Green functions on scales $\omega_m > \omega_N$ by tracing out intermediate degrees of freedom $e=(\alpha_{m+1},...,\alpha_N)$ in ϱ_N. Since the longest chain H_N is close to the infinite system limit, this should provide a better description of the spectra, particularly at higher frequencies. In order to carry out this procedure, the Hilbert space of each H_m is extended to that of H_N by adding the $N-m$ environment degrees of freedom e, see Fig. 9. Evaluating the reduced density matrix $\varrho^{\rm red}_m = {\rm Tr}_e\left[\varrho_N\right]$ appearing in Eq. (42) leads to a Lehmann representation for the spectral density at $T=0$

$$A_{d\sigma}(\omega,T=0) = \sum_{kk'} C^N_{kk'} M^N_{kk'}\,\delta\big(\omega-(E^N_\kappa - E^N_{k'})\big) \tag{50}$$

$$C^N_{kk'} = \sum_p \varrho^{\rm red}_{pk'} M^N_{p\kappa} + \sum_p \varrho^{\rm red}_{kp} M^N_{k'p} \tag{51}$$

in place of (46). In Fig. 10 we show a comparison of this approach with results from the

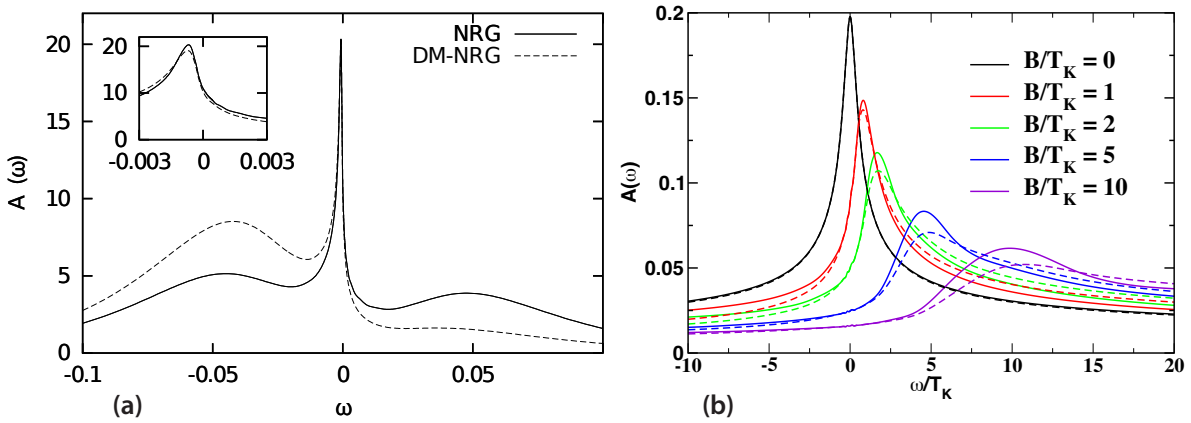

Fig. 10: *Spin-up spectral density $A(\omega, T = 0)$ for,* (**a**)*, the symmetric Anderson model, with $U/\Delta_0 = 10, \Delta_0 = 0.01$ and $B = \Delta_0/10$, with and without reduced density matrices (DM-NRG/NRG) [8], and,* (**b**)*, for the Kondo model in several magnetic fields B, with and without reduced density matrices (dashed/solid lines, respectively) [11,50], showing that the low-energy Kondo resonance is sufficiently well captured in the conventional approach.*

previous approach for the Anderson and Kondo models in a magnetic field. A field-induced rearrangement of spectral weight at $\omega \approx \varepsilon_d, \varepsilon_d + U$ is well captured by the reduced density matrix approach (Fig. 10a). The low-energy Kondo resonance is less subject to finite size corrections, since this part of the spectrum is already calculated from sufficiently long chains, such that the corrections in using reduced density matrices are small (Fig. 10b).

Transport properties

The transport properties of quantum impurity models require knowledge of both the frequency and temperature dependence of the impurity spectral density, a topic that was addressed above. The linear-response conductance $G(T)$ and thermopower $S(T)$ through a quantum dot described by the Anderson model are given by the following expressions

$$G(T) = \frac{e^2}{h} \int d\omega \left(-\frac{\partial f}{\partial \omega} \right) \sum_\sigma \mathcal{T}_\sigma(\omega, T, B) \,, \tag{52}$$

$$S(T) = -\frac{1}{|e|T} \frac{\int d\omega\, \omega \left(-\partial f/\partial\omega\right) \sum_\sigma \mathcal{T}_\sigma(\omega)}{\int d\omega \left(-\partial f/\partial\omega\right) \sum_\sigma \mathcal{T}_\sigma(\omega)} \,, \tag{53}$$

where the transmission function $\mathcal{T}_\sigma(\omega, T)$ through a quantum dot symmetrically coupled to left and right leads is related to $A_{d\sigma}(\omega, T)$ via

$$\mathcal{T}_\sigma(\omega, T) = 2\pi\Delta_0 A_{d\sigma}(\omega T) \,.$$

Note that the discrete form of the spectral function may be directly substituted into the expressions for $G(T)$ and $S(T)$ above without the necessity of broadening [51]. For the conductance, this leads to

$$G(T) = \frac{\gamma\beta}{Z} \sum_\sigma \sum_{m,n} |M^\sigma_{mn}|^2 \frac{1}{e^{\beta E_m} + e^{\beta E_n}} \,, \tag{54}$$

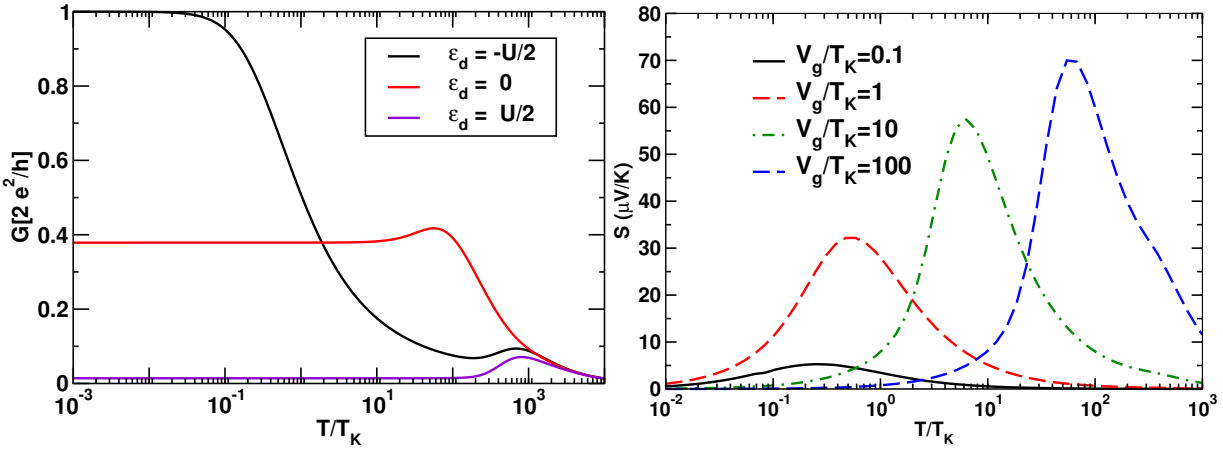

Fig. 11: *(**a**) Linear conductance $G(T)$ versus $T/T_{\rm K}$ for $U/\Delta_0 = 16$ and several values of $\varepsilon_d = -U/2,\ 0,\ +U/2$ using the approach of Yoshida et al. [51]. The resistivity of a Kondo impurity $\rho(T)$ is similar to $G(T)$ for the $\varepsilon_d = -U/2$ curve. NRG parameters were for $\Lambda = 4$, $n_z = 2$ [52]. (**b**). Thermopower of a negative $U = -16\Delta_0$ quantum dot, exhibiting a large enhancement for gate voltages $V_g \geq T_{\rm K}$ [53] (calculated within the full density matrix approach to spectral functions).*

with $\gamma = 2\pi\Delta_0\frac{e^2}{h}$. Results for the temperature dependence of the conductance of the Anderson model using this procedure are shown in Fig. 11a. Thermoelectric properties have also been investigated for quantum dots with repulsive onsite Coulomb interactions [54] and for attractive onsite interactions [53]. The latter provide a mechanism for enhancing thermopower, as shown in Fig. 11b. The method gives uniformly accurate results at high and low temperatures, as well as correctly describing the crossover region $T \approx T_{\rm K}$ (detailed comparisons of the resistivity of dilute magnetic impurities with known results at high and low temperature can be found in [7]). These calculations, as well as similar resistivity calculations for dilute impurities, provide a quantitative interpretation of experiments for $S = 1/2$ realizations of the Kondo effect. They have also been extended using the full density matrix approach to describe the resistivity and dephasing rates of real Fe impurities in Au and Ag by using a 3-channel Kondo model [35, 55].

5 Complete basis set and full density matrix

We noted in Sec. 3 that at each m, the states generated, denoted $|qm\rangle$, are partitioned into the lowest-energy retained states, denoted $|km\rangle$, and the high-energy eliminated (or discarded) states, $|lm\rangle$. In order to avoid an exponential increase in the dimension of the Hilbert space, only the former are used to set up and diagonalize the Hamiltonian for the next iteration $m+1$. The eliminated states, while not used in the iterative NRG procedure, may be used to set up a complete orthonormal basis set [12]. This complete basis set is very powerful and allows evaluating correlation functions $\langle A(t)B(0)\rangle$, transient quantities, and even thermodynamic expressions in an unambiguous way, avoiding any possible double counting of excitations. Eliminated states from different iterations have no overlap, see Fig. 12, in contrast to the retained states. Hence,

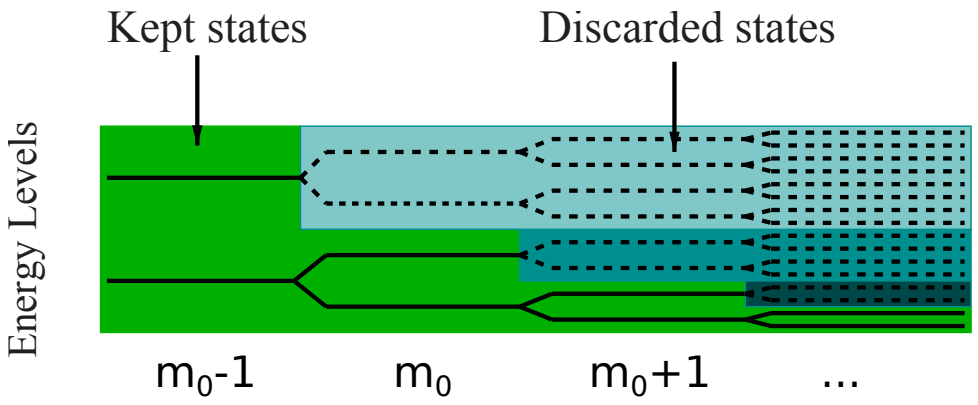

Fig. 12: *For iterations $m < m_0$ all states are kept, while for $m \geq m_0$ only the lowest* 1000 *or so states generated are used to set up the Hamiltonian for the next iteration $m + 1$ (adapted from [57]).*

using the latter to carry out calculations of physical quantities restricts one to using excitations from a single shell only. However, for finite-temperature Green functions and non-equilibrium quantities, multiple-shell contributions become important [56], and the complete basis set offers a way to evaluate these quantities [12].

The complete basis set is defined by the product states $|lem\rangle = |lm\rangle|e\rangle, m = m_0, \ldots, N$, where m_0 is the first iteration at which truncation occurs, and $|e\rangle = |\alpha_{m+1}\rangle|\alpha_{m+2}\rangle \ldots |\alpha_N\rangle$ are environment states at iteration m such that the product states $|lem\rangle$, for each $m = m_0, m_0 + 1, \ldots, N$, reside in the same Fock space (that of the largest system diagonalized, $m = N$). By "e" we shall henceforth denote the collection $e = \{\alpha_{m+1} ... \alpha_N\}$. The eliminated states satisfy the completeness relation [12, 58]

$$\sum_{m=m_0}^{N} \sum_{le} |lem\rangle\langle lem| = 1, \tag{55}$$

where for $m = N$ all states are counted as discarded (i.e., there are no kept states at iteration $m = N$). We shall also use the following representations of this relation [12, 58]

$$1 = 1_m^- + 1_m^+, \tag{56}$$

$$1_m^- = \sum_{m'=m_0}^{m} \sum_{l'e'} |l'e'm'\rangle\langle l'e'm'| \tag{57}$$

$$1_m^+ = \sum_{m'=m+1}^{N} \sum_{l'e'} |l'e'm'\rangle\langle l'e'm'| = \sum_{ke} |kem\rangle\langle kem| \,. \tag{58}$$

By using the complete basis set, we can construct the full density matrix FDM [10, 59]

$$\rho = \frac{1}{Z(T)} \sum_{m=m_0}^{N} \sum_{le} e^{-\beta E_l^m} |lem\rangle\langle lem|, \quad \mathrm{Tr}\,\rho = 1 \Rightarrow \tag{59}$$

$$Z(T) = \sum_{m=m_0}^{N} 4^{N-m} \sum_{l} e^{-\beta E_l^m} \equiv \sum_{m=m_0}^{N} 4^{N-m} Z_m(T) \tag{60}$$

where $Z(T)$ is the partition function made up of the complete spectrum, i.e., it contains the eliminated states from all H_m, $m = m_0, m_0+1, ..., N$. Consequently, it can be used to evaluate the impurity thermodynamics at arbitrary temperatures.
Consider the following density matrix for the m-th shell (defined, however, in the Hilbert space of H_N),

$$\tilde{\rho}_m = \sum_{le} |lem\rangle \frac{e^{-\beta E_l^m}}{\tilde{Z}_m} \langle lem| \,. \tag{61}$$

Normalization $Tr\,[\tilde{\rho}_m] = 1$ implies that

$$1 = \sum_l \frac{e^{-\beta E_l^m}}{\tilde{Z}_m}\, 4^{N-m} = 4^{N-m}\, \frac{Z_m}{\tilde{Z}_m}\,, \tag{62}$$

where $Z_m = \sum_l e^{-\beta E_l^m}$. Then the FDM can be written as a sum of weighted density matrices for shells $m = m_0, \ldots, N$

$$\rho = \sum_{m=m_0}^{N} w_m \tilde{\rho}_m \tag{63}$$

$$w_m = 4^{N-m}\, \frac{Z_m}{Z}\,; \quad \sum_{m=m_0}^{N} w_m = 1 \tag{64}$$

Application to thermodynamics

Substituting $\rho = \sum_m w_m \tilde{\rho}_m$ into the expression for the thermodynamic average $\langle \hat{O} \rangle$ of a local observable of the impurity (e.g., n_d or $n_{d\uparrow} n_{d\downarrow}$) and making use of the decomposition of unity Eq. (55), we have

$$\begin{aligned} \langle \hat{O} \rangle_\rho = \mathrm{Tr}\left[\rho \hat{O}\right] &= \sum_{l'e'm'} \left\langle l'e'm' \left| \hat{O} \sum_{lem} w_m \right| lem \right\rangle \frac{e^{-\beta E_l^m}}{\tilde{Z}_m} \langle lem | l'e'm' \rangle \\ = \sum_{lem} O_{ll}^m w_m \frac{e^{-\beta E_l^m}}{\tilde{Z}_m} &= \sum_{lm} 4^{N-m} w_m O_{ll}^m \frac{e^{-\beta E_l^m}}{4^{N-m} Z_m} = \sum_{m=m_0,l}^{N} w_m O_{ll}^m \frac{e^{-\beta E_l^m}}{Z_m}, \end{aligned} \tag{65}$$

where orthonormality $\langle lem | l'e'm' \rangle = \delta_{ll'} \delta_{ee'} \delta_{mm'}$, and the trace over the $N - m$ environment degrees of freedom $\sum_{lem} \cdots = \sum_{lm} 4^{N-m} \ldots$ has been used, and $O_{ll}^m = \langle lm | \hat{O} | lm \rangle$. For other observables, such as the specific heat or the susceptibility, one requires a similar calculation for the conduction band contribution $\langle \hat{O} \rangle_{\rho_0}$, with ρ_0 the FDM of the non-interacting band. The impurity contribution is then obtained as $O_{\mathrm{imp}} = \langle \hat{O} \rangle_\rho - \langle \hat{O} \rangle_{\rho_0}$.
For each temperature T and shell m, we require $w_m(T)$ and the factor $B_l^m(T) = e^{-\beta E_l^m}/Z_m$ where $Z_m = \sum_l e^{-\beta E_l^m}$. Numerical problems due to large exponentials are avoided by calculating $B_l^m(T) = e^{-\beta(E_l^m - E_0^m)}/Z'_m$ where $Z'_m = e^{\beta E_0^m} Z_m$ and E_0^m is the lowest discarded energy for shell m. Figure 13 shows results for the double occupancy of the Anderson model obtained within the FDM approach and comparisons with the conventional approach of Sec. 4.

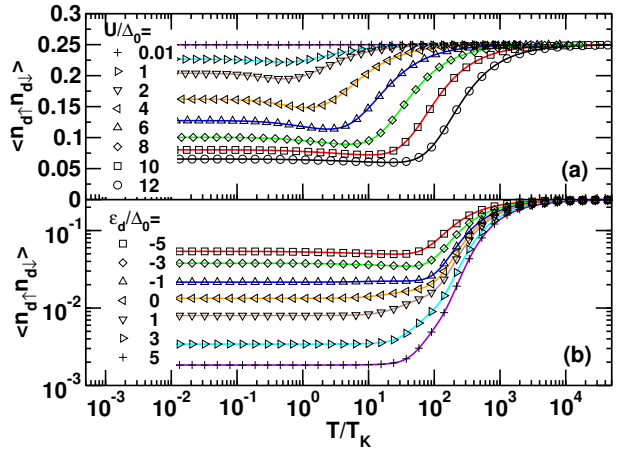

Fig. 13: *Double occupancy* $D_{\rm occ} = \langle n_{d\uparrow} n_{d\downarrow}\rangle$ *as a function of temperature* $T/T_{\rm K}$ *for, (a), the symmetric Anderson model at different* U/Δ_0*, and, (b), for the asymmetric Anderson model at* $U/\Delta_0 = 12$ *and increasing values of* $\varepsilon_d/\Delta_0 = -5, -3, -1, 0, +1, +3, +5$*. FDM (solid lines), conventional approach (symbols).* $\Lambda = 10$ *with* z*-averaging [*$n_z = 4$*,* $z = 1/8$*,* $1/2$*,* $3/8$*,* $3/4$*] [38].*

Application to dynamics

We consider a general fermionic/bosonic ($s = \pm 1$) retarded Green function

$$\begin{aligned} G_{AB}(t) = -i\theta(t)\langle [A(t), B]_s\rangle &\equiv -i\theta(t)\,{\rm Tr}\left[\rho(A(t)B + sBA(t))\right] \\ &= -i\theta(t)\left[C_{A(t)B} + sC_{BA(t)}\right], \end{aligned} \tag{66}$$

where A and B are fermionic/bosonic operators, e.g., for the d-level Green function of our quantum dot $A = d_\sigma$ and $B = d_\sigma^\dagger$. The trace is evaluated using the complete basis set. We outline the derivation of $C_{A(t)B}$, with the expression for $C_{BA(t)}$ obtained in a similar manner. We have

$$\begin{aligned} C_{A(t)B} = {\rm Tr}\left[\rho A(t)B\right] &= \sum_{lem} \langle lem|e^{iHt}Ae^{-iHt}B\rho|lem\rangle \\ &= \sum_{lem}\sum_{l'e'm'} \langle lem|e^{iHt}Ae^{-iHt}|l'e'm'\rangle\langle l'e'm'|B\rho|lem\rangle\,, \end{aligned} \tag{67}$$

which consists of three contributions with $m' = m$, $m' > m$ and $m' < m$. Consider the first contribution ($m' = m$), denoted by $C^{(i)}_{A(t)B}$. Using the NRG approximation $e^{-iHt}\,|l'e'm\rangle \approx e^{-iH_m t}\,|l'e'm\rangle = e^{-iE^m_{l'}t}\,|l'e'm\rangle$ and $\langle lem|A|l'e'm\rangle = \delta_{ee'}\langle lm|A|l'm\rangle = \delta_{ee'}A^m_{ll'}$, we have

$$C^{(i)}_{A(t)B} = \sum_{lm}\sum_{l'} e^{-i(E^m_{l'}-E^m_l)t}A^m_{ll'}\sum_e \underbrace{\langle l'em|B\rho|lem\rangle}_{(B\rho)^m_{l'e,le}}\,.$$

Inserting the FDM expression $\rho = \sum_m w_m\tilde{\rho}_m$ into $(B\rho)^m_{l'e,le}$ yields

$$\sum_e (B\rho)^m_{l'e,le} = B^m_{l'l}w_m e^{-\beta E^m_l}/Z_m\,,$$

hence we have

$$C^{(i)}_{A(t)B} = \sum_m \frac{w_m}{Z_m}\sum_l\sum_{l'} e^{-i(E^m_{l'}-E^m_l)t}A^m_{ll'}B^m_{l'l}e^{-\beta E^m_l}. \tag{68}$$

The off-diagonal contributions with $m' > m$ and $m' < m$ in Eq. (67), which we label by $C^{(ii)}_{A(t)B}$ and $C^{(iii)}_{A(t)B}$, may be put into diagonal form by using $1^+_m = \sum_{m'=m+1}^N \sum_{l'e'} |l'e'm'\rangle\langle l'e'm'| =$

$\sum_{ke}|kem\rangle\langle kem|$ [Eq. (58)], thereby introducing kept states at iteration m (or m') in place of discarded states at iterations $m' > m$ (or $m > m'$),

$$\begin{aligned}
C^{(ii)}_{A(t)B} &= \sum_{l'e'm'>m}\sum_{lem}\langle lem|e^{iHt}Ae^{-iHt}|l'e'm'\rangle\langle l'e'm'|B\rho|lem\rangle \\
&= \sum_{lem}\sum_{ke'}\langle lem|e^{iHt}Ae^{-iHt}|ke'm\rangle\langle ke'm|B\rho|lem\rangle \\
&\approx \sum_{lm}\sum_{k} e^{-i(E^m_k-E^m_l)t}A^m_{lk}\sum_e (B\rho)^m_{ke,le} \\
&= \sum_{lm}\sum_{k} e^{-i(E^m_k-E^m_l)t}A^m_{lk}B^m_{kl}e^{-\beta E^m_l}\frac{w_m}{Z_m} \qquad (69)\\
C^{(iii)}_{A(t)B} &= \sum_{lem>m'}\sum_{l'e'm'}\langle lem|e^{iHt}Ae^{-iHt}|l'e'm'\rangle\langle l'e'm'|B\rho|lem\rangle \\
&= \sum_{l'e'm'}\sum_{ke'}\langle l'e'm'|B\rho|ke'm\rangle\langle ke'm|e^{iHt}Ae^{-iHt}|l'e'm'\rangle \\
&\approx \sum_{l'm'}(B\rho)_{l'e',ke'}e^{-i(E^{m'}_{l'}-E^{m'}_k)t}A^{m'}_{kl'} \qquad (70)
\end{aligned}$$

where the NRG approximation has been used together with $\sum_e (B\rho)^m_{ke,le} = B^m_{kl}e^{-\beta E^m_l}\frac{w_m}{Z_m}$. It is also easy to show that [54],

$$\mathrm{Tr}_e\left[(B\rho)^m_{le,ke}\right] \equiv \sum_e (B\rho)^m_{le,ke} = \sum_{k'} B^m_{lk'}\underbrace{\sum_e\langle k'em|\rho|kem\rangle}_{R^m_{\rm red}(k',k)} \qquad (71)$$

where $R^m_{\rm red}(k',k)$ is the reduced density matrix obtained from the FDM ρ by tracing out the degrees of freedom $e = (\alpha_{m+1},...,\alpha_N)$ [10, 54], hence the contribution $C^{(iii)}_{A(t)B}$ may be written as

$$C^{(iii)}_{A(t)B} = \sum_{lm}(B\rho)_{le,ke}e^{-i(E^m_l-E^m_k)t}A^m_{kl} = \sum_{lkk'm} e^{-i(E^m_l-E^m_k)t}A^m_{kl}B^m_{lk'}R^m_{\rm red}(k',k), \qquad (72)$$

and

$$\begin{aligned}
C_{A(t)B} = C^{(i)}_{A(t)B} + C^{(ii)}_{A(t)B} + C^{(iii)}_{A(t)B} &= \sum_m\frac{w_m}{Z_m}\sum_{ll'} e^{-i(E^m_{l'}-E^m_l)t}A^m_{ll'}B^m_{l'l}e^{-\beta E^m_l} \\
&+ \sum_m\frac{w_m}{Z_m}\sum_{lk} e^{-i(E^m_k-E^m_l)t}A^m_{lk}B^m_{kl}e^{-\beta E^m_l} \qquad (73)\\
&+ \sum_m\sum_{lkk'} e^{-i(E^m_l-E^m_k)t}A^m_{kl}B^m_{lk'}R^m_{\rm red}(k',k)\,.
\end{aligned}$$

Similar arguments lead to an expression for $C_{BA(t)}$ (exercise),

$$\begin{aligned}
C_{BA(t)} = C^{(i)}_{BA(t)} + C^{(ii)}_{BA(t)} + C^{(iii)}_{BA(t)} &= \sum_m\frac{w_m}{Z_m}\sum_{ll'} e^{-i(E^m_{l'}-E^m_l)t}A^m_{ll'}B^m_{l'l}e^{-\beta E^m_{l'}} \\
&+ \sum_m\frac{w_m}{Z_m}\sum_{lk} e^{-i(E^m_l-E^m_k)t}A^m_{kl}B^m_{lk}e^{-\beta E^m_l} \qquad (74)\\
&+ \sum_m\sum_{lkk'} e^{-i(E^m_k-E^m_l)t}A^m_{lk}B^m_{k'l}R^m_{\rm red}(k,k')\,.
\end{aligned}$$

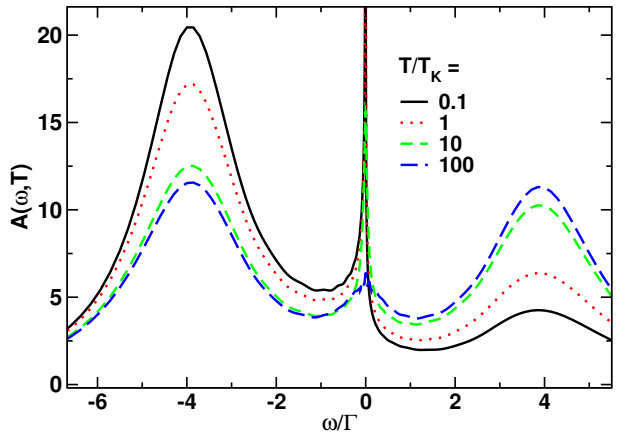

Fig. 14: *Spectral function of a negative-U quantum dot modeled by the Anderson model with $U/\Gamma = -8$ at finite gate voltage $V_g = T_{\rm K}$ and several temperatures, calculated within the FDM approach (adapted from [53]). The spectral function, polarized at low temperatures, becomes unpolarized at $T \gg T_{\rm K}$.*

Fourier transforming $-i\theta(t)(C_{A(t)B} + sC_{BA(t)})$ using

$$\int_{-\infty}^{+\infty} -i\theta(t) e^{-i(E_{q'}-E_q)} e^{i(\omega+i\delta)} = 1/(\omega + i\delta - (E_{q'} - E_q)) \tag{75}$$

finally yields the Green function

$$\begin{aligned} G_{AB}(\omega+i\delta) = & \sum_{m=m_0}^{N} \frac{w_m}{Z_m} \sum_{ll'} A^m_{ll'} B^m_{l'l} \frac{e^{-\beta E^m_l} + s e^{-\beta E^m_{l'}}}{\omega + i\delta - (E^m_{l'} - E^m_l)} \\ & + \sum_{m=m_0}^{N-1} \frac{w_m}{Z_m} \sum_{lk} A^m_{lk} B^m_{kl} \frac{e^{-\beta E^m_l}}{\omega + i\delta - (E^m_k - E^m_l)} \\ & + s \sum_{m=m_0}^{N-1} \frac{w_m}{Z_m} \sum_{lk} A^m_{kl} B^m_{lk} \frac{e^{-\beta E^m_l}}{\omega + i\delta - (E^m_l - E^m_k)} \\ & + \sum_{m=m_0}^{N-1} \sum_{lkk'} A^m_{kl} B^m_{lk'} \frac{R^m_{\rm red}(k',k)}{\omega + i\delta - (E^m_l - E^m_k)} \\ & + s \sum_{m=m_0}^{N-1} \sum_{lkk'} A^m_{lk} B^m_{k'l} \frac{R^m_{\rm red}(k,k')}{\omega + i\delta - (E^m_k - E^m_l)} \,. \end{aligned} \tag{76}$$

The reduced density matrices appearing in Eq. (76) can be evaluated efficiently at all temperatures in a recursive manner [10]. The use of the complete basis set to calculate finite-temperature Green functions ensures that the spectral sum rule $\int d\omega\, A_\sigma(\omega, T) = 1$ holds as an identity [10]. Furthermore, calculations at $\omega < T$ may be carried out without the need to restrict to a smaller cluster $M < N$, as was the case with the approach described in Sec. 4. Fig. 14 shows the spectral function of the negative-U Anderson model calculated from Eq. (76) at several temperatures.

For an application of this approach to thermoelectric properties of quantum dots see Ref. [54], and for a recent application to the magnetoresistivity and dephasing rate of multi-channel Kondo models see Ref. [35].

6 Recent developments: TDNRG and multiorbital Kondo physics

The NRG has proved to be a reliable method for dealing with equilibrium properties of strongly correlated quantum impurity systems. Nevertheless, the method is still under development. In this section, we describe two areas where significant progress has been made but where further work is needed. The first is in the transient response of a quantum impurity following either a quantum quench, a pulse of finite duration, or a periodic train of pulses [12, 56, 58, 60, 61]. This is relevant, for example, in many pump-probe experiments [62, 63]. The second area is in developing ways to deal with real quantum impurities in metals or on surfaces, such as impurities with partially filled d- or f-levels, in which multiple channels (or bands) of the host may couple to the impurity.

Time-dependent NRG (TDNRG)

We are interested in the dynamics of a local observable $\hat{O}$ following a quantum quench in which one or more system parameters of H change suddenly at $t = 0$. Thus, the time-dependence of H is described by $H(t) = \theta(-t)H^i + \theta(t)H^f$, with H^i and H^f being time-independent initial ($t < 0$) and final state ($t > 0$) Hamiltonians, respectively [56]. The time evolution of $\hat{O}$ at $t > 0$ is then given by $O(t) = \mathrm{Tr}\left[\rho(t)\hat{O}\right]$ where $\rho(t) = e^{-iH^f t}\rho\, e^{iH^f t}$ is the time-evolved density matrix and $\rho = e^{-\beta H^i}/\mathrm{Tr}\,[\rho]$ is the density matrix of the initial state at inverse temperature β. In terms of the complete basis set, we have

$$\begin{aligned} O(t) = Tr\left[e^{-iH^f t}\rho\, e^{iH^f t}\hat{O}\right] &= \sum_{m=m_0}^{N}\sum_{le} {}_f\langle lem|e^{-iH^f t}\rho\, e^{iH^f t}\hat{O}|lem\rangle_f \\ &= \sum_{mm'=m_0}^{N}\sum_{lel'e'} {}_f\langle lem|e^{-iH^f t}\rho\, e^{iH^f t}|l'e'm'\rangle_f\ {}_f\langle l'e'm'|\hat{O}|lem\rangle_f\,. \end{aligned} \tag{77}$$

Making use of $1_m^+ = \sum_{m'=m+1}^{N}\sum_{l'e'}|l'e'm'\rangle\langle l'e'm'| = \sum_{ke}|kem\rangle\langle\, kem|$ [Eq. (58)], allows us to write [12]

$$\begin{aligned} O(t) &= \sum_{m=m_0}^{N}\sum_{rs\notin KK'}\sum_{e} {}_f\langle sem|e^{-iH^f t}\rho\, e^{iH^f t}|rem\rangle_f\ {}_f\langle rem|\hat{O}|sem\rangle_f \\ &\approx \sum_{m=m_0}^{N}\sum_{rs\notin KK'}\sum_{e} {}_f\langle sem|e^{-iH^f_m t}\rho\, e^{iH^f_m t}|rem\rangle_f\ {}_f\langle rem|\hat{O}|sem\rangle_f \\ &= \sum_{m=m_0}^{N}\sum_{rs\notin KK'}\Big(\sum_{e} {}_f\langle sem|\rho|rem\rangle_f\Big)e^{-i(E^m_s-E^m_r)t}O^m_{rs} \\ &= \sum_{m=m_0}^{N}\sum_{rs\notin KK'}\rho^{i\to f}_{sr}(m)e^{-i(E^m_s-E^m_r)t}O^m_{rs}\,, \end{aligned} \tag{78}$$

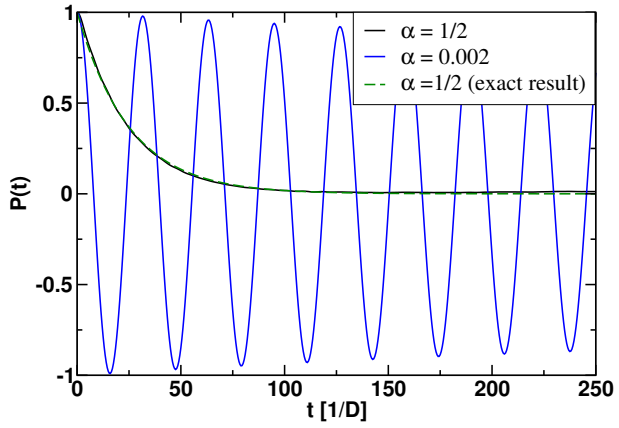

Fig. 15: $P(t) = \langle\sigma_z(t)\rangle$ *of the IRLM (with* $\sigma_z = 2n_d - 1$*) using the TDNRG as formulated in Ref. [60]. In the initial state* $\varepsilon_d = -\infty$ *so that* $P(t \leq 0) = +1$*, while in the final state at* $t > 0$ *the level is shifted to* $\varepsilon_d = 0$ *so that the two-level system can relax to its new groundstate. For weak dissipation* $\alpha \ll 1$*, one observes weakly damped coherent oscillations. These vanish for* $\alpha \geq 1/2$*. The NRG parameters used are* $\Lambda = 4$*,* $n_z = 32$ *with resonant level width* $\Gamma = 0.02\,D$*, where* $D = 1$ *is the half-width of the IRLM (and a semi-elliptic density of states was used).*

in which r and s may not both be kept states, $O^m_{rs} = {}_f\langle lem|\hat{O}|rem\rangle_f$ are the final state matrix elements of $\hat{O}$, which are independent of e, the NRG approximation

$$H^f|rem\rangle \approx H^f_m|rem\rangle = E^m_r|rem\rangle, \tag{79}$$

is adopted [in the second line of Eq. (78)], and $\rho^{i\to f}_{sr}(m) = \sum_e {}_f\langle sem|\rho|rem\rangle_f$ represents the reduced density matrix of the initial state projected onto the basis of final states (henceforth called the *projected density matrix*). The latter has been evaluated for the special choice of a density matrix defined on the longest Wilson chain

$$\rho = \sum_l |lN\rangle_i \frac{e^{-\beta E^N_l}}{Z_N} {}_i\langle lN|, \tag{80}$$

with $Z_N = \sum_l e^{-\beta E^N_l}$, in which only the discarded states of the last NRG iteration enter [12,58]. More recently, the projected density matrix has been evaluated for a general initial density matrix, given by the full density matrix of the initial state [60]. This allows calculations to be carried out at arbitrary finite temperature. While the short-time limit $O(t \to 0^\dagger)$ in the TDNRG recovers the exact thermodynamic value $O^i = \mathrm{Tr}\,[\rho O]$ in the initial state, the long-time limit suffers from an error of a few percent. In addition, significant noise is observed at intermediate $t\Gamma \gtrsim 1$ to long times $t\Gamma \gg 1$. Attempts to further improve the method may be found in Ref. [60] and references therein. A generalization of the single-quench TDNRG formalism to multiple quenches, allowing applications to systems subject to general pulses or periodic driving fields, may be found in Ref. [61]. Figure 15 shows results for the quantity $P(t) = \langle\sigma_z(t)\rangle$ of the ohmic spin boson model (calculated via the IRLM using the equivalence between models discussed earlier). The aforementioned error of a few percent in the long time limit is evident in the case $\alpha = 1/2$, whose exact result is $P(t) = e^{-2\Gamma t}$. This is likely due to the finite heat capacity of the logarithmically discretized bath, which implies that the energy change following a quench cannot be fully dissipated into such a bath [64].

Multi-orbital and multi-channel Kondo models

The Anderson impurity model is a starting point for describing many different systems, from the classic examples of transition-metal magnetic impurities such as Fe or Mn in non-magnetic metals such as Au, to rare-earth magnetic impurities in non-magnetic metals, such as Ce in $LaAl_2$ [26] or magnetic ions such as Co, Fe and Ti adsorbed on surfaces of non-magnetic metals such as Cu or Cu_2N/Cu (where the Cu_2N monolayer reduces the hybridization V to the substrate [66]). Of course, the relevant correlated orbitals in these systems are not the non-degenerate "s-levels" as in (3), but would be the 5-fold or 7-fold degenerate partially filled d- or f-orbitals in the case of transition metal or rare earth metal impurities, respectively. Furthermore, electrons in these partially filled shells would be subject to Coulomb, Hund's exchange, spin-orbit and crystal-field interactions, often leading to non-degenerate low-energy multiplets. In addition, these low-energy multiplets would hybridize with conduction channels of appropriate symmetry, and in general with many channels, not just one as in (3). Such a non-degenerate multi-channel Anderson model capable of describing a real transition-metal impurity would then look more complicated than Eq. (3), e.g., the following model (but still neglecting spin-orbit and crystal field interactions),

$$
\begin{aligned}
H = & \sum_{m\sigma} \varepsilon_{dm}\, n_{m\sigma} + \frac{U}{2}\sum_{m\sigma} n_{m\sigma}n_{m-\sigma} + \frac{U'}{2}\sum_{m\neq m'\sigma} n_{m\sigma}n_{m'-\sigma} + \frac{U'-J}{2}\sum_{m\neq m'\sigma} n_{m\sigma}n_{m'\sigma} \\
& - \frac{J}{2}\sum_{m\neq m'\sigma} d^\dagger_{m\sigma}d_{m-\sigma}d^\dagger_{m'-\sigma}d_{m'\sigma} - \frac{J'}{2}\sum_{m\neq m'\sigma} d^\dagger_{m\sigma}d^\dagger_{m-\sigma}d_{m'-\sigma}d_{m'\sigma} \\
& + \sum_{km\sigma} \epsilon_{km\sigma}\, c^\dagger_{km\sigma}c_{km\sigma} + \sum_{km\sigma} V_{km\sigma}(c^\dagger_{km\sigma}d_{m\sigma} + h.c.)
\end{aligned}
$$

would be closer to describing a real transition-metal impurity such as Mn in Cu. Despite its apparent complexity, this model, just like its simpler counterpart in Eq. (3), has the same general structure as Eq. (2) describing a general quantum impurity model, namely all many-body interactions (U, U', J, J') are contained in a local part $H_{\rm imp}$, while the multi-channel bath $H_{\rm bath}$ represents non-interacting electrons coupling via a one-body hybridization to $H_{\rm imp}$. While the NRG can be applied to such multi-channel models, for N_c-channels the Hilbert space grows as 4^{N_c} instead of 4 as for a single channel. The fraction of states that can be retained at each iteration is correspondingly smaller $(1/4^{N_c})$ than for a single channel $(1/4)$, making accurate calculations difficult, particularly for dynamical quantities. While implementing all available symmetries $(U(1), SU(2), SU(3)$, parity etc.), in order to increase the fraction of states that can be retained at each iteration, will help, such symmetries are not always present. At present, reliable NRG calculations for dynamics can be carried out for three-channel models [35]. It should be emphasized that the difficulty is with the number of channels that couple to the impurity, not the complexity or number of orbitals on the impurity. Thus, while resistivity calculations for three-channel fully screened Kondo models, such as those shown in Fig. 16a, are demanding and require full use of all available symmetries, it is relatively straightforward to deal with underscreened Kondo models [67] with high spin values, as shown in Fig. 16b

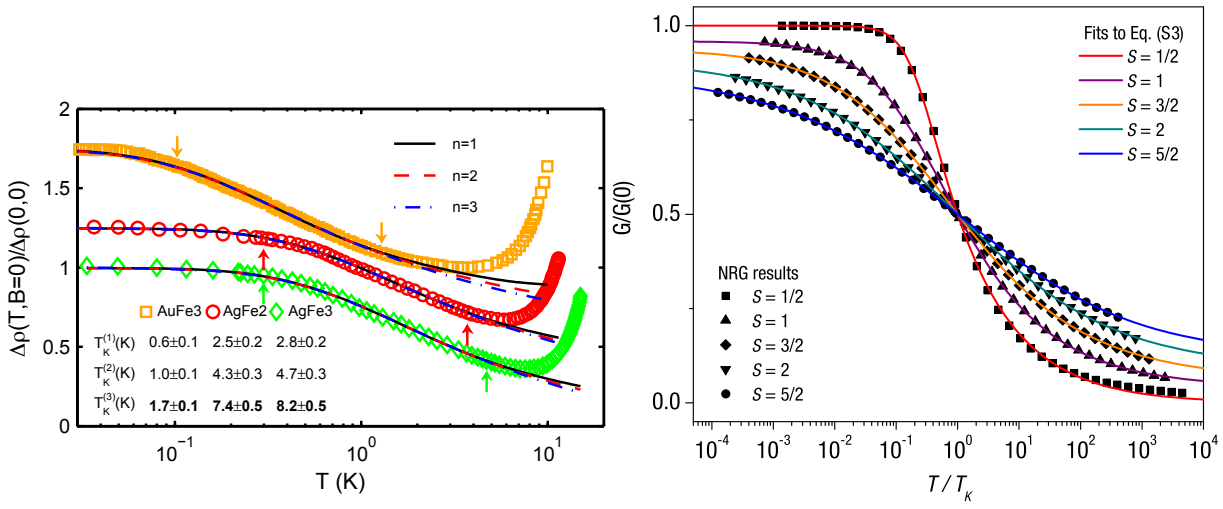

Fig. 16: *Temperature dependence of, (a), the Kondo resistivity of one, two and three-channel fully screened Kondo models compared to experimental data for the Kondo contribution $\Delta\rho$ to the resistivity of Fe impurities in Au and Ag [35, 55]. Consistency in the extracted Kondo scales $T_{\rm K}^n$ for resistivity and dephasing measurements allows one to conclude that only the $S = 3/2$ three-channel Kondo model could fit all experimental data. (b), conductance curves $G(T)$ for $S > 1/2$ single-channel underscreened Kondo models (contrasted with the fully screened $S = 1/2$ case) from Ref. [65].*

for the resistivity curves for the single-channel underscreened Kondo model [65, 68]. Increasing the number of channels to five would be a significant development, allowing many interesting realistic systems to be investigated with NRG in combination with *ab-initio* methods to extract the relevant model parameters [55, 69, 70]. We mention here one recent proposal for achieving this, which, however, has so far only been benchmarked on a three-channel model [71]. As in the single-band case, we rewrite the above model in linear-chain form with $H_{\rm bath} = \sum_{m=1}^{N_c} \sum_{k\sigma} \epsilon_{km\sigma}\, c^\dagger_{km\sigma} c_{km\sigma} \to \sum_{m=1}^{N_c} \sum_{n=0}^{\infty} \sum_\sigma t_{mn} (f^\dagger_{mn\sigma} f_{mn+1\sigma} + H.c.)$, where $t_{mn} \sim D_m \Lambda^{-n/2}, m = 1, ..., N_c$ for N_c channels with half-bandwidths D_m. If all channels have the same half-bandwidth $D_m = D, m = 1, ..., N_c$, the hoppings within a shell $t_{mn}, m = 1, ..., N_c$ are constant, one has to add all orbitals $f_{mn+1\sigma}, m = 1, ..., N_c$ of the next shell $n + 1$ in going from H_n to H_{n+1} in the NRG procedure of Sec. 3 before truncating the spectrum of H_{n+1}, hence leading to the above growth of the Hilbert space at each iteration. Choosing band-widths D_m with $D_1 > D_2 > ... > D_{N_c}$, as suggested in Ref. [71], leads to an energy scale separation of the orbitals within each shell, i.e., $t_{mn} \sim D_m \Lambda^{-n/2}$ for fixed n decrease with $m = 1, ..., N_c$. This allows adding the orbitals $f_{mn+1\sigma}, m = 1, ..., N_c$ of a given shell sequentially while simultaneously truncating the spectrum after each orbital is added. The calculation then resembles a single-channel calculation. The above energy scale separation is guaranteed provided $D_m/D_{m+1} = 1/g = \Lambda^{-1/2N_c}$, implying $t_{m+1n}/t_{mn} = g < 1$. Since the hoppings in this approach decrease by a factor $\Lambda^{-1/2N_c}$, a larger Λ will be required to obtain the same accuracy as a single-channel calculation. In this way, the authors obtained accurate results for three-channel and three-impurity models.

7 Summary

Wilson's non-perturbative NRG transformation for the Kondo model has become a powerful tool for the study of quantum impurity models in general. It gives information on the many-body eigenvalues and eigenstates of such models on all energy scales and thereby allows the direct calculation of their thermodynamic, dynamic, and transport properties. Recently, it has been further developed to yield the transient response of these systems to a sudden perturbation (a quantum quench) [12], the time-dependent NRG (TDNRG). Extensions of the TDNRG to general pulses using multiple quenches have also been made [60, 61]. The NRG also has potential to give information on the non-equilibrium steady-state transport through correlated impurity systems such as quantum dots. Recent work tries to construct a non-equilibrium density matrix for such systems by using the TDNRG to time-evolve from a known initial density matrix [72].
The method has been extended in new directions, such as to models with bosonic baths to study spin-boson models [27] and the interplay of correlations and phonon effects in Anderson-Holstein models [73]. It has also been used successfully to make progress on understanding the Mott transition, heavy fermion behavior, and other phenomena in correlated lattice systems [42, 74–76]. There is room for further improvement and extensions of the method both technically and in the investigation of more complex systems such as multi-impurity and multi-channel models [35, 71, 77].

Acknowledgement

Useful discussions with R. Bulla, H. Nghiem, L. Merker, D. Kennes and V. Meden are acknowledged (as is use of figures from joint work). Many relevant papers have not been cited in these lecture notes and we apologize to the authors for this. For a more comprehensive survey of the literature on NRG work, see Ref. [4].

Appendices

A Logarithmic discretization approximation

The approximation

$$H_c = \int_{-1}^{+1} d\varepsilon\, \varepsilon\, c^\dagger_{\varepsilon\sigma} c_{\varepsilon\sigma} \approx \sum_{n=0}^{\infty} \left(\varepsilon_{-n}\, c^\dagger_{-n\sigma} c_{-n\sigma} + \varepsilon_{+n}\, c^\dagger_{+n\sigma} c_{+n\sigma} \right) \tag{81}$$

used to replace the continuum band by the discrete one can be analyzed by introducing a complete orthonormal basis set of states for the conduction electrons in each interval $\pm[\Lambda^{-(n+1)}, \Lambda^{-n}]$ using the following wavefunctions

$$\psi^{\pm}_{np}(\varepsilon) = \begin{cases} \frac{\Lambda^{n/2}}{(1-\Lambda^{-1})^{1/2}}\, e^{\pm i\omega_n p\varepsilon} & \text{for } \Lambda^{-(n+1)} < \pm\varepsilon < \Lambda^{-n} \\ 0 & \text{otherwise} \end{cases} \tag{82}$$

Here p is a Fourier harmonic index and $\omega_n = 2\pi\Lambda^n/(1-\Lambda^{-1})$. The operators $c_{\varepsilon\sigma}$ can be expanded in terms of a complete set of new operators $a_{np\sigma}, b_{np\sigma}$ labeled by the interval n and the harmonic index p

$$c_{\varepsilon\sigma} = \sum_{np} \left[a_{np\sigma}\, \psi^{+}_{np}(\varepsilon) + b_{np\sigma}\, \psi^{-}_{np}(\varepsilon) \right]. \tag{83}$$

In terms of these operators, the Kondo Hamiltonian becomes

$$\begin{aligned} H_{KM} &= \frac{1}{2}\left(1+\Lambda^{-1}\right) \sum_{np} \Lambda^{-n} \left(a^\dagger_{np\sigma} a_{np\sigma} - b^\dagger_{np\sigma} b_{np\sigma} \right) \\ &+ \frac{(1-\Lambda^{-1})}{2\pi i} \sum_{n} \sum_{p\neq p'} \Lambda^{-n} \left(a^\dagger_{np\sigma} a_{np'\sigma} - b^\dagger_{np\sigma} b_{np'\sigma} \right) e^{\frac{2\pi i(p-p')}{1-\Lambda^{-1}}} \\ &+ J \sum_{\sigma\sigma'} f^\dagger_{0\sigma}\, \vec{\sigma}_{\sigma\sigma'}\, f_{0\sigma'} \cdot \vec{S}\,, \end{aligned} \tag{84}$$

where in terms of the new operators, $f_{0\sigma} = \frac{1}{\sqrt{2}} \int_{-1}^{+1} d\varepsilon\, c_{\varepsilon\sigma}$ contains only $p = 0$ states:

$$f_{0\sigma} = \frac{1}{\sqrt{2}} \int_{-1}^{+1} d\varepsilon\, c_{\varepsilon\sigma} = \left[\frac{1}{2}(1-\Lambda^{-1}) \right]^{1/2} \sum_{n=0}^{\infty} \Lambda^{-n/2} \left(a_{n0\sigma} + b_{n0\sigma} \right). \tag{85}$$

We notice that only the $p = 0$ harmonic appears in the local Wannier state. This is a consequence of the assumption that the Kondo exchange is independent of k. Hence the conduction electron orbitals a_{np}, b_{np} for $p \neq 0$ only couple to the impurity spin indirectly via their coupling to the a_{n0}, b_{n0} in the second term of Eq. (84). This coupling is weak, being proportional to $(1-\Lambda^{-1})$, and vanishes in the continuum limit $\Lambda \longrightarrow 1$, so these states may be expected to contribute little to the impurity properties compared to the $p = 0$ states. This is indeed the case as shown by explicit calculations in [1, 2]. The logarithmic discretization approximation consists of neglecting conduction electron states with $p \neq 0$, resulting in H_c given by Eq. (81) with $c_{+n\sigma} \equiv a_{n,0\sigma}$ and $c_{-n\sigma} \equiv b_{n,0\sigma}$ and a discrete Kondo Hamiltonian given by Eq. (10).

B Lanczos procedure

Neglecting spin indices, the conduction electron operator is

$$H_c = \sum_k \varepsilon_k \, c_k^\dagger c_k \, .$$

The Lanczos algorithm for tridiagonalizing this operator by repeated action on the normalized conduction electron Wannier state $|0\rangle = \frac{1}{\sqrt{N}} \sum_k c_k^\dagger |vac\rangle$, with $|vac\rangle$ the vacuum state and N the number of sites in the crystal, is

$$|1\rangle = \frac{1}{t_0}\big(H_c|0\rangle - |0\rangle\langle 0|H_c|0\rangle\big) \tag{86}$$

$$|n+1\rangle = \frac{1}{t_n}\big(H_c|n\rangle - |n\rangle\langle n|H_c|n\rangle - |n-1\rangle\langle n-1|H_c|n\rangle\big) \tag{87}$$

yielding

$$H_c = \sum_{n=0}^{\infty} \epsilon_n \, f_n^\dagger f_n + t_n \left(f_n^\dagger f_{n+1} + H.c.\right), \tag{88}$$

where the site energies are given by $\epsilon_n = \langle n|H_c|n\rangle$ and the hoppings t_n are obtained as normalizations from Eqs. (86)-(87).

References

[1] K.G. Wilson, Rev. Mod. Phys. **47**, 773 (1975)

[2] H.R. Krishna-murthy, J.W. Wilkins, and K.G. Wilson, Phys. Rev. B **21**, 1003 (1980)

[3] H.R. Krishna-murthy, J.W. Wilkins, and K.G. Wilson, Phys. Rev. B **21**, 1044 (1980)

[4] R. Bulla, T.A. Costi, and T. Pruschke, Rev. Mod. Phys. **80**, 395 (2008)

[5] H.O. Frota and L.N. Oliveira, Phys. Rev. B **33**, 7871 (1986)

[6] T.A. Costi and A.C. Hewson, Philosophical Magazine Part B **65**, 1165 (1992)

[7] T.A. Costi, A.C. Hewson, and V. Zlatić, J. Phys.: Condens. Matter **6**, 2519 (1994)

[8] W. Hofstetter, Phys. Rev. Lett. **85**, 1508 (2000)

[9] R. Peters, T. Pruschke, and F.B. Anders, Phys. Rev. B **74**, 245114 (2006)

[10] A. Weichselbaum and J. von Delft, Phys. Rev. Lett. **99**, 076402 (2007)

[11] T.A. Costi, Phys. Rev. Lett. **85**, 1504 (2000)

[12] F.B. Anders and A. Schiller, Phys. Rev. Lett. **95**, 196801 (2005)

[13] B.A. Jones, C.M. Varma, and J.W. Wilkins, Phys. Rev. Lett. **61**, 125 (1988)

[14] A.J. Leggett, S. Chakravarty, A.T. Dorsey, M.P.A. Fisher, A. Garg, and W. Zwerger, Rev. Mod. Phys. **59**, 1 (1987)

[15] U. Weiss: *Quantum dissipative systems*, Vol. 13 (World Scientific Pub Co Inc, 2008)

[16] A. Georges, G. Kotliar, W. Krauth, and M.J. Rozenberg, Rev. Mod. Phys. **68**, 13 (1996)

[17] W. de Haas, J. de Boer, and G. van den Berg, Physica **1**, 1115 (1934)

[18] P.W. Anderson, Phys. Rev. **124**, 41 (1961)

[19] P.W. Anderson, Journal of Physics C: Solid State Physics **3**, 2436 (1970)

[20] R. Bulla, T. Pruschke, and A.C. Hewson, Journal of Physics: Condensed Matter **9**, 10463 (1997)

[21] C. Gonzalez-Buxton and K. Ingersent, Phys. Rev. B **57**, 14254 (1998)

[22] D. Goldhaber-Gordon, H. Shtrikman, D. Mahalu, D. Abusch-Magder, U. Meirav, and M.A. Kastner, Nature **391**, 156 (1998)

[23] D. Goldhaber-Gordon, J. Göres, M.A. Kastner, H. Shtrikman, D. Mahalu, and U. Meirav, Phys. Rev. Lett. **81**, 5225 (1998)

[24] S.R. White, Phys. Rev. Lett. **69**, 2863 (1992)

[25] U. Schollwöck, Rev. Mod. Phys. **77**, 259 (2005)

[26] A.C. Hewson: *The Kondo Problem to Heavy Fermions* (Cambridge Univ. Press, 1997)

[27] R. Bulla, H.-J. Lee, N.-H. Tong, and M. Vojta, Phys. Rev. B **71**, 045122 (2005)

[28] J. von Delft and H. Schoeller, Annalen der Physik **7**, 225 (1998)

[29] F. Guinea, V. Hakim, and A. Muramatsu, Phys. Rev. B **32**, 4410 (1985)

[30] T.A. Costi and C. Kieffer, Phys. Rev. Lett. **76**, 1683 (1996)

[31] T.A. Costi and G. Zarand, Physical Review B **59**, 12398 (1999)

[32] F. Lesage and H. Saleur, Phys. Rev. Lett. **80**, 4370 (1998)

[33] F. Verstraete, V. Murg, and J.I. Cirac, Advances in Physics **57**, 143 (2008)

[34] A. Weichselbaum, Annals of Physics **327**, 2972 (2012)

[35] M. Hanl, A. Weichselbaum, T.A. Costi, F. Mallet, L. Saminadayar, C. Bäuerle, and J. von Delft, Phys. Rev. B **88**, 075146 (2013)

[36] L. Borda, Phys. Rev. B **75**, 041307 (2007)

[37] L. Merker and T.A. Costi, Phys. Rev. B **86**, 075150 (2012)

[38] L. Merker, A. Weichselbaum, and T.A. Costi, Phys. Rev. B **86**, 075153 (2012)

[39] W.C. Oliveira and L.N. Oliveira, Phys. Rev. B **49**, 11986 (1994)

[40] V.L. Campo and L.N. Oliveira, Phys. Rev. B **72**, 104432 (2005)

[41] O. Sakai, Y. Shimizu, and T. Kasuya,
Journal of the Physical Society of Japan **58**, 3666 (1989)

[42] R. Bulla, T.A. Costi, and D. Vollhardt, Phys. Rev. B **64**, 045103 (2001)

[43] A. Freyn and S. Florens, Phys. Rev. B **79**, 121102 (2009)

[44] R. Zitko, Computer Physics Communications **180**, 1271 (2009)

[45] R. Zitko and T. Pruschke, Phys. Rev. B **79**, 085106 (2009)

[46] W. Metzner and D. Vollhardt, Phys. Rev. Lett. **62**, 324 (1989)

[47] G. Kotliar and D. Vollhardt, Physics Today **57**, 53 (2004)

[48] D. Vollhardt, Annalen der Physik **524**, 1 (2012)

[49] M. Yoshida, M.A. Whitaker, and L.N. Oliveira, Phys. Rev. B **41**, 9403 (1990)

[50] T.A. Costi, eprint arXiv:cond-mat/0212651 (2002)

[51] M. Yoshida, A.C. Seridonio, and L.N. Oliveira, Phys. Rev. B **80**, 235317 (2009)

[52] L. Merker, S. Kirchner, E. Muñoz, and T.A. Costi, Phys. Rev. B **87**, 165132 (2013)

[53] S. Andergassen, T.A. Costi, and V. Zlatić, Phys. Rev. B **84**, 241107 (2011)

[54] T.A. Costi and V. Zlatić, Phys. Rev. B **81**, 235127 (2010)

[55] T.A. Costi, L. Bergqvist, A. Weichselbaum, J. von Delft, T. Micklitz, A. Rosch, P. Mavropoulos, P.H. Dederichs, F. Mallet, L. Saminadayar, and C. Bäuerle, Phys. Rev. Lett. **102**, 056802 (2009)

[56] T.A. Costi, Phys. Rev. B **55**, 3003 (1997)

[57] A.I. Tóth, C.P. Moca, O. Legeza, and G. Zaránd, Phys. Rev. B **78**, 245109 (2008)

[58] F.B. Anders and A. Schiller, Phys. Rev. B **74**, 245113 (2006)

[59] A. Weichselbaum, Phys. Rev. B **86**, 245124 (2012)

[60] H.T.M. Nghiem and T.A. Costi, Phys. Rev. B **89**, 075118 (2014)

[61] H.T.M. Nghiem and T.A. Costi, Phys. Rev. B **90**, 035129 (2014)

[62] L. Perfetti, P.A. Loukakos, M. Lisowski, U. Bovensiepen, H. Berger, S. Biermann, P.S. Cornaglia, A. Georges, and M. Wolf, Phys. Rev. Lett. **97**, 067402 (2006)

[63] S. Loth, M. Etzkorn, C.P. Lutz, D.M. Eigler, and A.J. Heinrich, Science **329**, 1628 (2010)

[64] A. Rosch, The European Physical Journal B **85**, 1 (2012)

[65] J.J. Parks, A.R. Champagne, T.A. Costi, W.W. Shum, A.N. Pasupathy, E. Neuscamman, S. Flores-Torres, P.S. Cornaglia, A.A. Aligia, C.A. Balseiro, G.K.-L. Chan, H.D. Abruña, and D.C. Ralph, Science **328**, 1370 (2010)

[66] A. Otte, M. Ternes, K. Von Bergmann, S. Loth, H. Brune, C. Lutz, C. Hirjibehedin, and A. Heinrich, Nature Physics **4**, 847 (2008)

[67] A. Posazhennikova and P. Coleman, Phys. Rev. Lett. **94**, 036802 (2005)

[68] N. Roch, S. Florens, T.A. Costi, W. Wernsdorfer, and F. Balestro, Phys. Rev. Lett. **103**, 197202 (2009)

[69] P. Lucignano, R. Mazzarello, A. Smogunov, M. Fabrizio, and E. Tosatti, Nature Materials **8**, 563 (2009)

[70] R. Requist, S. Modesti, P.P. Baruselli, A. Smogunov, M. Fabrizio, and E. Tosatti, Proceedings of the National Academy of Sciences pp. 69–74 (2013)

[71] A.K. Mitchell, M.R. Galpin, S. Wilson-Fletcher, D.E. Logan, and R. Bulla, Phys. Rev. B 89, 121105 (2014)

[72] F.B. Anders, Phys. Rev. Lett. **101**, 066804 (2008)

[73] D. Meyer, A.C. Hewson, and R. Bulla, Phys. Rev. Lett. **89**, 196401 (2002)

[74] R. Bulla, Phys. Rev. Lett. **83**, 136 (1999)

[75] T.A. Costi and N. Manini, Journal of Low Temperature Physics **126**, 835 (2002).

[76] W. Koller, D. Meyer, and A.C. Hewson, Phys. Rev. B **70**, 155103 (2004)

[77] T. Pruschke and R. Bulla, The European Physical Journal B **44**, 217 (2005)